# AN ENERGY ABSORPTION INVESTIGATION OF CFRP COMPOSITE THIN-WALLED TUBES WITH PVC FOAM-FILLED CORES

A Thesis

Presented in Partial Fulfillment of the Requirements for the

Degree of Master of Science

with a

Major in Civil Engineering

in the

College of Graduate Studies

University of Idaho

by

Lucas de Lemos Coutinho

Major Professor: Ahmed A. Ibrahim, Ph.D., P.E.

Committee Members: Richard J. Nielsen, Ph.D., P.E.; Kevin Chang, Ph.D., P.E.

Department Chair: Patricia J. S. Colberg, Ph.D., P.E.

May 2021

# AUHORIZATION TO SUBMIT THESIS

This thesis of Lucas de Lemos Coutinho, submitted for the degree of Master of Science with a Major in Civil Engineering and titled "AN ENERGY ABSORPTION INVESTIGATION OF CFRP COMPOSITE THIN-WALLED TUBES WITH PVC FOAM-FILLED CORES," has been reviewed in final form. Permission, as indicated by the signatures and dates below, is now granted to submit final copies to the College of Graduate Studies for approval.

Major Professor: _____ Date: 4-12-2021
Ahmed A. Ibrahim, Ph.D., P.E.

Committee Members: _____ Date: 13 April, 2021
Richard J. Nielsen, Ph.D., P.E.

_____ Date: 4-12-21
Kevin Chang, Ph.D., P.E.

Department Chair: _____ Date: 4-18-21
Patricia J. S. Colberg, Ph.D., P.E.

# ABSTRACT

Today, thin-walled (TW) structures are known for their use in several fields such as aerospace, automotive, rail, and maritime. With the growing concern for life-threatening terrorist attacks, these structures have been studied for their use in structural engineering as well, as part of protective structural systems. With the goal of achieving excellent crashworthiness performance with the minimum possible weight, systems comprised of lightweight materials with high strength-to-weight properties are subjects of study. The primary objective of this study is to investigate the effect of carbon fiber reinforced polymers (CFRP) and polyvinyl chloride (PVC) foam reinforcements on the crashworthiness of tall, thin-walled circular aluminum tubes, to be used as energy absorbers. This investigation was done by experimentally testing tubes with inner diameter of 60 mm, wall thickness of 1.6 mm, and 120 mm in length with different reinforcement configurations under quasi-static axial loads. The effect of epoxy on energy absorption capability was investigated to determine whether adhesives are to be used to bond the tube wall and the foam core or not. In addition, tubes with CFRP and PVC foam reinforcing configuration and varying lengths (40 mm, 80 mm, and 120 mm) were tested to determine the most efficient configuration with tubes of different length-to-diameter ratios (L/D).

The study concluded that CFRP and PVC foam reinforcements increase the energy absorption of tall aluminum tubes by 37% and the peak force by 20% compared to the control, unreinforced, aluminum tubes. Also, these reinforcements were found to have complementary effects on energy absorption capabilities of aluminum tubes. Although epoxy adhesion between the foam core and tube wall was found to increase the peak load by 2%, it does not improve energy absorption while increasing the mass of the specimen by 9%. The CFRP and PVC foam reinforcing configuration was found to be equally effective for tubes between 80 mm (L/D = 1.33) and 120 mm (L/D = 2.00) with a proportional increase in energy absorption with an increased length. However, it was found that the smaller the specimen, the higher the peak load.

**Keywords:** Crashworthiness, composite materials, sandwich cores, carbon fiber reinforced polymer, foam-filled tubes, energy absorption, PVC foam, axial load, structural retrofitting

# ACKNOWLEDGEMENTS

# DEDICATION

To my grandfather, Hélio Coutinho da Silva, I wish to express my gratitude for all his efforts and for the influence he had in my life. I am truly blessed to have had him by my side during all my life achievements and each of these would not have been possible without his support and encouragement. Without him I neither would be the person I am today nor I would be where I am today. I especially dedicate this work to him, to my father, Hélio, my mother, Lígia, my sister, Laís, and my grandmothers for their unconditional love and support throughout my studies.

# TABLE OF CONTENTS

# LIST OF TABLES

# LIST OF FIGURES

# CHAPTER 1: INTRODUCTION

## 1.1 PROBLEM STATEMENT

Over the past decades, there has been a growing concern for life-threatening terrorist attacks. Explosions within or nearby buildings generate blast waves, which may cause localized shear or flexural failure in the closest structural members [1]. Various forms of danger to people are expected from these incidents; from the overpressure and heat of the explosion, to falling debris and structural collapse. Examples of these events are the Oklahoma City bombing in 1995 [2], the Islamabad Marriott Hotel bombing in 2008 [3], and the Nashville bombing in 2020 [4], which combined, caused more than 220 fatalities. In addition to these intentional blasts, other accidental detonations have occurred with the Beirut's ammonium nitrate blast in 2020 being the most notable recent event [5]. These and many other tragic events, not only cause numerous fatalities, but also have economical and unmeasurable societal impact. Regardless of the detonation source or causes, it is necessary to protect facilities to mitigate consequential impacts and preserve human lives.

Because conventional structures are rarely designed to resist blast loads, it is necessary to find options to retrofit these structures against these kind of loads. Protective structures such as sacrificial cladding structures are adopted to minimize the potential impact of detonation hazards. Efficient mitigation systems are generally made of sandwich panels [6] composed of three layers. These layers are usually made of metals or composite materials, where outer panels have the function of evenly transferring the applied pressure to the core, which is responsible for absorbing the energy. Because the energy absorption efficiency of the system relies on its inner layer, this core is the most critical component of sandwich structures and is the main target of crashworthiness investigations.

The retrofit of structures through sacrificial cladding installation requires excellent crashworthiness performance with the lightest possible materials. This is because this cladding must be able to minimize the potential damage to the main structural components and protect occupants from detonation debris. At the same time, it should not substantially affect the weight of the building as its members are not initially designed for such additional load. Luckily, with the continuous improvement of current materials and creation of new ones, there is an increasing variety of high-strength, lightweight engineered materials. Examples of these

materials are fiber reinforced polymers (FRPs) and foams. In addition to showing high strength-to-weight ratios, these materials can be easily installed and allow freedom in design. Because of these attractive parameters, these materials have shown to be useful in the retrofit of multiple structural elements, including their use as reinforcing materials for sandwich panel cores.

## 1.2 OBJECTIVE OF RESEARCH

The primary objective of this study was to investigate the effects of carbon fiber reinforced polymers (CFRP) and polyvinyl chloride (PVC) foam reinforcements on the crashworthiness of thin-walled (TW) circular aluminum tubes. First, the effects of foam-filled core adhesives on the energy absorption capability of aluminum tubes were investigated by quasi-statically compressing specimens with epoxied and non-epoxied foam-filled cores. Then, specimens with different combinations of reinforcements were tested to investigate their failure mechanisms, and compare their crashworthiness quantities. Finally, the influence of different length-to-diameter (L/D) ratios on the crashworthiness of reinforced tubes was investigated by testing specimens with different lengths.

A secondary objective of this study was to develop conclusions on the best specimen configuration between the analyzed reinforcement combinations and the L/D ratio to be used in sandwich panel cores or other energy absorption systems. This includes the consideration of performance, constructability, cost, and weight of the materials.

## 1.3 THESIS OUTLINE

The thesis is divided into four chapters (Chapters 2-5) which present an analysis of energy absorption capabilities of TW aluminum tubes in combination with CFRP and PVC foam reinforcements.

**Chapter 2:** "LITERATURE REVIEW": This chapter summarizes relevant and current research on thin-walled aluminum tubes for energy absorption applications and the use of FRP and foam core reinforcements.

**Chapter 3:** "EXPERIMENTAL PROGRAM": This chapter explains the specimen preparation and experimental procedures along with the materials used and their properties.

**Chapter 4:** "RESULTS AND DISCUSSIONS": This chapter presents the axial compression test results for the various developed specimens. Also, the findings are discussed.

**Chapter 5:** "CONCLUSIONS AND RECOMMENDATIONS": This chapter presents the conclusions from the investigation (Chapter 4) and provides recommendations for future research on this topic.

# CHAPTER 2: LITERATURE REVIEW

## 2.1 INTRODUCTION

Crashworthiness is the ability of a structure to absorb impact energy while collapsing in a progressive and predictable manner [7]. This controlled failure is ideal as it significantly decreases the force experienced by the occupants in the event of a blast [8]. Although this characteristic is generally associated with industries such as aerospace, automotive, rail, and maritime, this concept is of high importance in civil engineering structures as well. When these structures are subjected to blast loading, the collapse of the load bearing components such as beams and columns can cause major human casualties. Therefore, a solution is required to inhibit collapse. One alternative is the use of sacrificial cladding, which is usually made of sandwich panels composed of two outer panels and an inner energy absorbing core [6, 9] as shown in Figure 2-1.
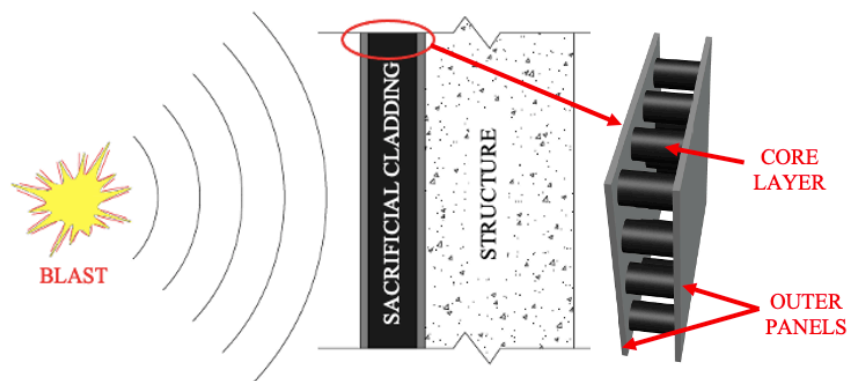


**Figure 2-1: Sacrificial cladding schematic**

The escalating interest in the improvement and refinement of structural crashworthiness has resulted in a significant amount of research on this topic. TW metallic tubes have been widely investigated for their crushing behavior and application as energy absorbers. These are the most common structural elements used for energy absorption due to their high strength-to-weight ratio, relatively low costs, and high energy absorption efficiency. As first shown by Alexander et al. [10] in 1960, this kind of structure absorbs the crushing energy nearly at a constant load. Aluminum alloys and mild steel are the most common materials used for TW tubes due to their ductility, which allows these metals to diffuse the imposed energy by

generating a stable and progressive plastic deformation. Under axial compression, it is possible to predict the deformation behavior these materials will exhibit in real-life applications due to the consistency and foreseen characteristics of these tubes.

## 2.2 AXIAL LOAD TESTING

Through axial compression tests, it is possible to measure the ability of a specimen to withstand or absorb imposed energy. There are two different methods of conducting axial crushing tests: impact and quasi-static testing. Each of these tests simulate a different loading characteristic of the material and can be imposed in real-life applications.

### 2.2.1 Impact Testing

An impact loading dynamic test is carried out by using a drop hammer or an impactor. An impact test setup is seen in Figure 2-2. This test is used to determine the crashworthiness ability of a material when a sudden load is imposed to it. To avoid buckling failure during this test, it is necessary to perform a set of iterative calculations, to determine the tube geometry and dimensions. Tubes subjected to this test can be of different shapes such as round, square, hexagonal, cones, or plates. Specimens usually have lengths between 50 and 120 mm, an outer diameter of 20-100 mm, and a wall thickness of 1-3 mm [11]. Since this test requires advanced equipment to collect and analyze the data such as displacement laser sensors, a high-speed camera for slow motion analysis, an accelerometer, and remote controllers, this test is relatively expensive. Because of this, quasi-static testing is being used instead.

### 2.2.2 Quasi-Static Testing

A quasi-static test is carried out by axially compressing the specimen between a dynamic and a static plate at low and constant crosshead speeds, between the range of $1.5\times10^{-3}$ and 0.1 m/s [7]. Unlike the impact test, this test does not quite simulate a real blast load because the force is not applied with the same strain rate as a real blast test. In spite of this, it is possible to observe failure mechanisms and energy absorption quantities by generating compression load versus displacement curves of the specimen [12]. The quasi-static test setup is seen in Figure 2-3.
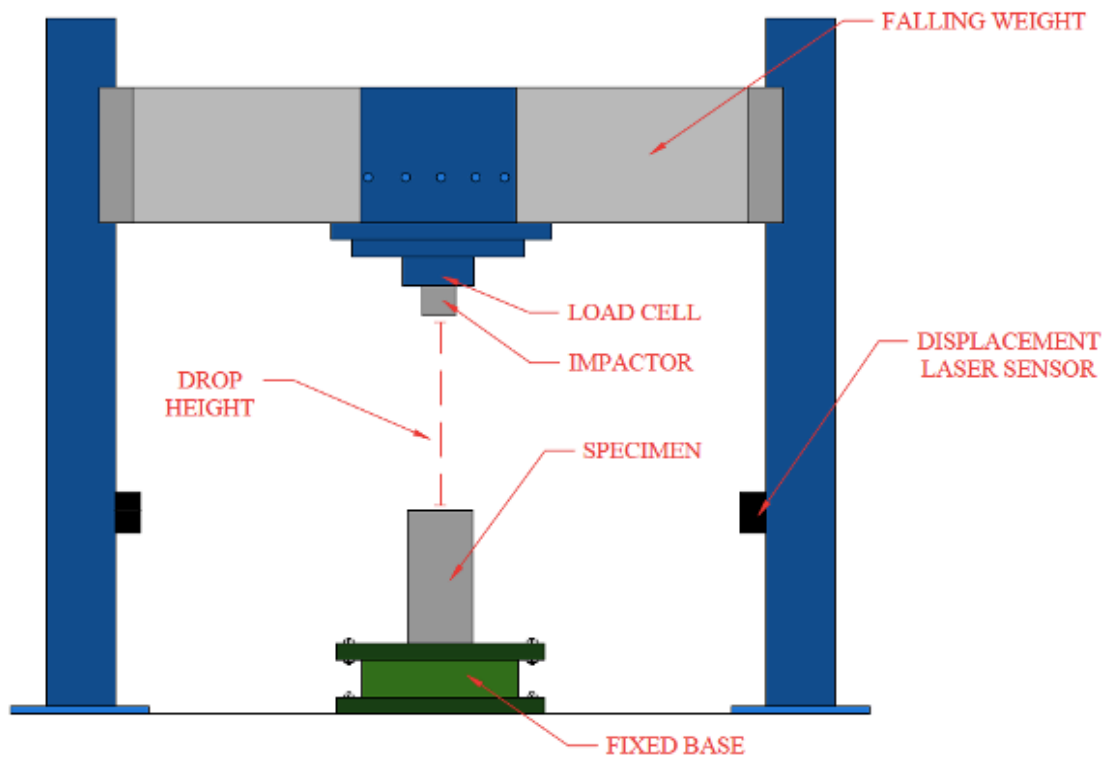
**Figure 2-2: Impact test setup**
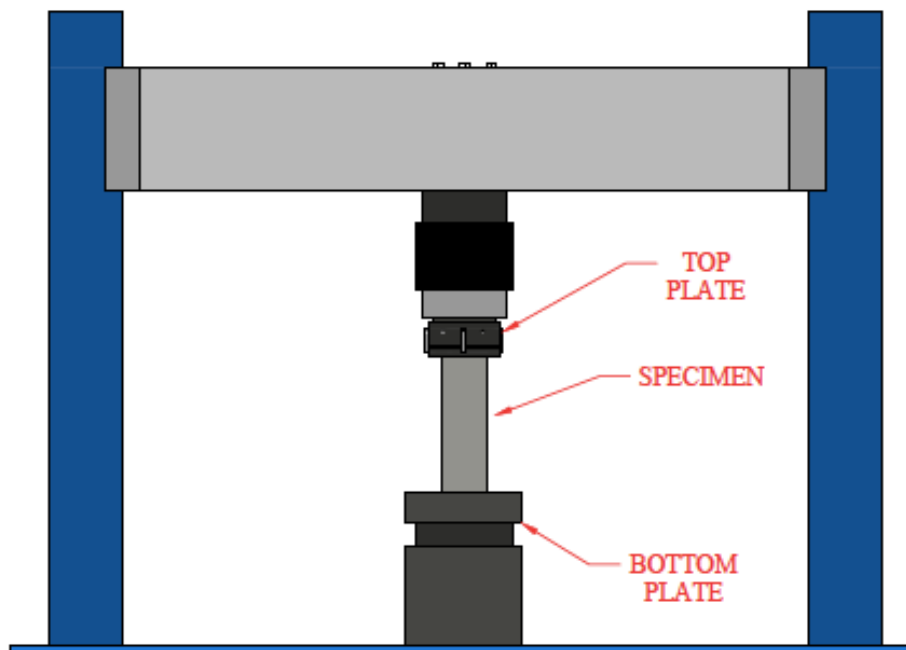


**Figure 2-3: Quasi-static test setup**

## 2.3 CRASHWORTHINESS ANALYSIS

The energy absorption capability of a specimen is determined experimentally by investigating its crashworthiness quantities and by analyzing its failure mechanism.

### 2.3.1 Crashworthiness Quantities

The energy absorption capability quantities of a specimen are calculated from the load versus displacement history, which can be generated from either impact or quasi-static testing. An illustrative plot is shown in Figure 2-4, which it can be divided into three different zones with respect to the x-axis. The pre-crushing or linear elastic zone (I) is the initial region and is from the origin to the peak load ($P_{max}$), which is the maximum load neglecting the compaction zone. From $P_{max}$, the post-crushing or plateau region (II) is observed. This region is characterized by the average crushing load ($P_{avg}$). After the post-crushing zone, the compaction or densification region (III) is observed and can be neglected in the design phase [13]. Various crashworthiness quantities can be derived from the following plot as discussed below.
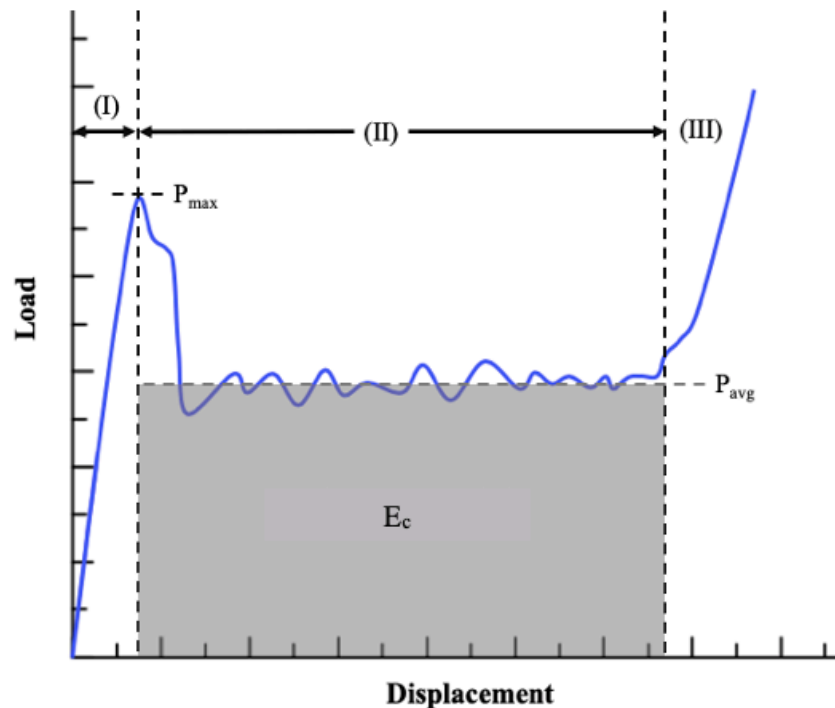


**Figure 2-4: Illustrative load-displacement curve**

$P_{max}$ is defined as the maximum load observed in a test and is the highest load required to cause critical and irreversible deformation to the specimen [14]. The total absorbed energy (*EA*), in J, is the area under the load-displacement curve. Therefore,

$$EA = \int_0^{\Delta max} Pd\Delta \qquad \text{(Equation I)}$$

Where P is the crushing load in kN and $\Delta$ is the displacement in mm. The specific absorbed energy (SEA), in J/grams, is defined as the absorbed crushing energy per unit mass of the specimen. Therefore,

$$SEA = \frac{EA}{m} \qquad \text{(Equation II)}$$

Where m is the mass of the crushed specimen in grams. To determine $P_{avg}$, the following calculation can be performed.

$$P_{avg} = \frac{E_c}{\Delta_c} \qquad \text{(Equation III)}$$

where $E_c$ is the energy absorbed or the area under the curve in the plateau region, seen in Figure 2-4 and $\Delta_c$ is the post-crushing displacement or the displacement experienced during the plateau region. Another important quantity to be derived is the crushing force efficiency (CFE), which is the ratio of $P_{avg}$ and $P_{max}$ [13].

## 2.3.2 Failure Mechanisms

The crashworthiness of a specimen is also evaluated by observing the failure mechanism of the specimen subjected to the compression load. A crashworthy structure should absorb the imposed energy through progressive crushing in a controlled manner [13]. The collapse mode can be either catastrophic or progressive [11]. Illustrative load versus displacement histories for each of these failures are seen in Figure 2-5.
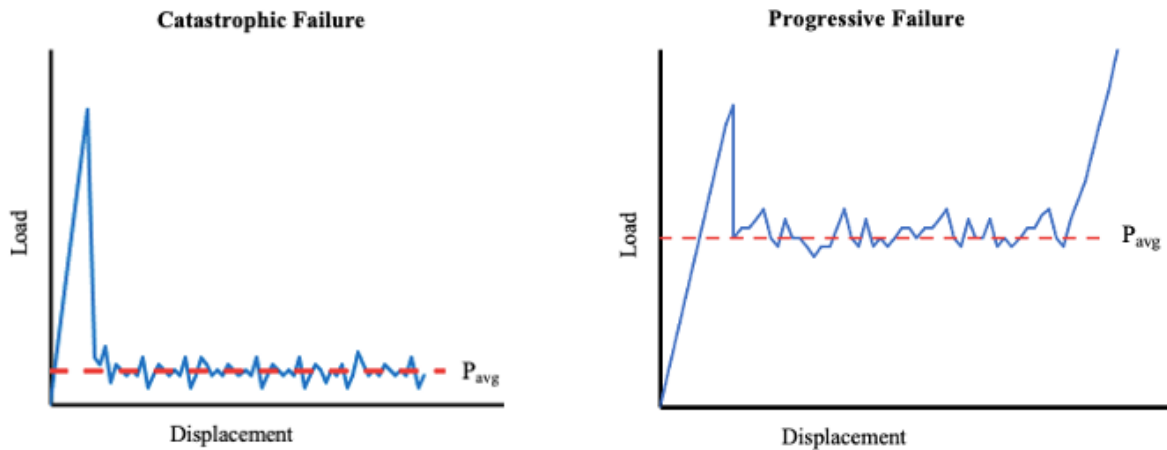
**Figure 2-5: Catastrophic versus progressive collapse**

As seen, a catastrophic failure results in sudden drop of load after the peak load is imposed. Therefore, it has a smaller area under the load-displacement curve, which means that lower energy is absorbed. This kind of failure is often associated with buckling. On the other hand, progressive failure is ideal since the plateau region of the graph is at a much higher load, which means that the specimen absorbs more energy. There are three potential progressive failure modes for aluminum tubes: axisymmetric (concertina), diamond, and mixed modes. Figure 2-6 illustrates the concertina and the diamond modes. The mixed mode is a combination of these failure modes.
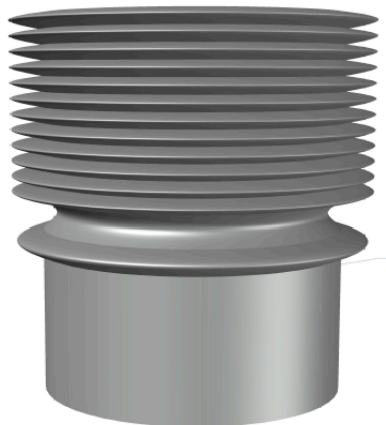


(a)                          (b)

**Figure 2-6: Typical deformation modes of circular aluminum tubes under axial load, (a) concertina mode, (b) diamond mode**

Hollow aluminum tubes tend to suffer diamond or mixed modes [7] due to the wall deformation and these folding mechanisms change with the L/D ratios and by the diameter-to-wall thickness ratios (D/t) [15]. By contrast, foam reinforcement, tends to fail in a concertina mode [7]. With CFRP reinforcement, more sophisticated deformation modes tend to occur as noted by Abada et al. [16]. It was observed that progressive crushing was accompanied by the formation of fronds, as seen in Figure 2-7, that propagate outwards, which correspond to the types of stable brittle failure of composites called "splaying" and "lamina bending". When the peak load was achieved, the progressive failure modes of the specimens were commenced with crack formations parallel to the longitudinal axis which yielded local stress concentration [16].



**Figure 2-7: Fronds in CFRP reinforced tubes**

## 2.4 SPECIMEN MATERIALS AND APPLICATIONS

Numerous studies have been conducted to assess the energy absorption capability of TW structures. These tubes can have various cross-sectional shapes such as circular, square, octagonal, hexagonal, and corrugated [17, 18, 19]. TW structures with sinusoidal, tapered and straight shapes have also been explored [17, 18, 19, 20]. Tubular structures are preferable rather than any other cross-sectional shape due to their high strength-to-weight ratio and their ability to dissipate the imposed axial load through a progressive deformation [21]. One alternative is to increase the wall thickness of the specimen [22, 23]. However, this increases the weight of the material as well, which is a disadvantage.

Another alternative is to fill the specimen's core with honeycomb or to weld stiffeners to tie the opposite quadrants of the specimen as shown in Figure 2-8.
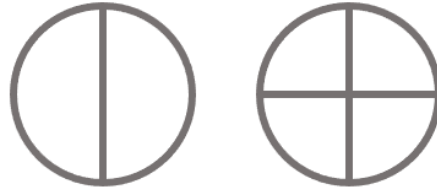


**Figure 2-8: Illustrative tubes with stiffeners**

Abada et al. [16] quasi-statically compressed aluminum tubes of 60 mm inner diameter, 120 mm height, and 1.6 mm wall thickness under a rate of 8 mm/min, and found that a quadruple-cell structure has higher energy absorption capacity compared to single-cell (hollow) and double-cell aluminum tubes. However, similarly to the increase in wall thickness of the specimens, the addition of stiffeners yields in an increase in specimen weight. Also, it is difficult to produce aluminum double or quadruple-cell tubes due to material characteristics of strain concentration and low ductility [24]. Additionally, this material requires relatively high electrical energy and large-size facilities to weld the tubes [24]. Alternatively, lighter and non-corrosive materials can be used in combination with the metallic tubes to achieve a similar or higher energy absorption capacity with less weight. By combining the tube material with other lightweight materials, a composite structure is formed, which improves the original tube material properties and, as a result, can increase the specific energy absorption capability of the specimen. Examples of lightweight materials that can be used either together or exclusively are FRPs and foam reinforcements.

## 2.4.1 Aluminum Tubes

Aluminum is the most abundant metal on Earth, representing 8% of its crust [25]. However, aluminum needs to be extracted from oxide, which is a very energy intensive process. In fact, 2-3% of the electricity used in the United States is consumed in the production process of this material [25]. Steel and aluminum have been widely used in many structural engineering applications because they can be easily formed in various shapes and joined together [7] and

are the most common materials used for energy absorption applications. Though similar, these materials are very different in some ways and these differences are worth noting. Aluminum is corrosion resistant without any further treatment. Differently, steel needs to be painted or treated to protect it from corrosion. Also, aluminum is more elastic, which allows it to be created in shapes that steel cannot. It is known that steel, wood, and concrete are the major construction materials. Aluminum, however, has not been extensively used as primary structural components in construction. In fact, approximately 0.000015% (9 out of 600,000) of the bridges in the United States have aluminum as the primary structural members [25]. This is mainly because it has a relatively high initial cost in these applications. Since the modulus of elasticity of aluminum is only about one-third that of steel [25], the sizes and structural dimensions of aluminum members must be larger than steel members to provide the same structural capacity. Because of these factors, aluminum is mainly used in structures as architectural components. On the other hand, it accounts for 80% of the structural weight of aircrafts and is a popular material in the automotive industry [25]. Aluminum alloys are used for these applications due to their corrosion resistance, light weight (it has one-third the density of steel), energy absorption capability [7, 21, 26, 27] and their relatively high specific strength [26]. The round tube selected for this research was aluminum alloy 6061-T6. This grade is highly versatile and normally used for aerospace, marine, and structural applications due to its good strength-to-weight ratio, above average corrosion resistance, good machinability, and excellent welding capability [28].

## 2.4.2 Fiber Reinforced Polymers

FRP materials are composed of high-strength fibers bonded with a polymer matrix (polyesters, vinylesters, or epoxies) [29], which protects fibers and enables them to act together in transferring the applied loads [30]. Although these materials have been used in the automotive and aerospace for more than 60 years [29], they also have been used as a construction material for structural strengthening in the United States for about 30 years [30]. Several factors have drawn the attention of building owners and engineers to these materials with cost, performance, and aesthetics being the major material selection parameters. As composite materials, FRPs have higher strength-to-weight ratio than steel reinforcement (rebar) and can be installed quickly and easily, which decreases labor costs [30]. Along with the cost-

effectiveness of these materials, FRPs are non-corrosive, which not only protects the structure, but also yields in a higher capacity over time when compared to other materials, and allows them to be used in a wide variety of environments [29]. Additionally, FRPs have low thermal conductivity and are electromagnetically neutral. This can be a critical factor in certain special structures that require little or no electromagnetic interference [29] such as some structures that store life support machines or military assets designed for electronic warfare. Because the use of FRPs as construction material is relatively new, some limitations are involved. The bond between the FRP system and the reinforcing structure is critical; therefore specialized labor is required. Proper mixing technique, surface preparation, material application, and curing process are crucial for these materials to perform at their potential [30].

### 2.4.2.1 CFRP Reinforcement

Although composite materials can also be formed with epoxy-impregnated glass fiber or Kevlar [31], CFRP systems are the most common FRP systems [30]. This is due to their superior mechanical properties and higher tensile strength, durability, and stiffness compared to other fiber systems [30]. Carbon fiber is one of the strongest most lightweight materials on the market [32] and is five times stronger and three times lighter than steel [32]. This material is usually sold into sheets and is classified into woven and non-woven. Weave is critical when selecting the desired fabric due their different appearances and functionalities [32]. The most common woven sheets are plain weave, harness satin weave, and twill weave [33] which are shown in Figure 2-9. Woven fabrics are classified into the number of fibers per tow (strands twisted together) [32]. 3k, 6k, and 12k are available fabrics, which have 3000, 6000, and 12,000 strands of carbon in each tow, respectively.



(a)　　　　　　　　　(b)　　　　　　　　　(c)
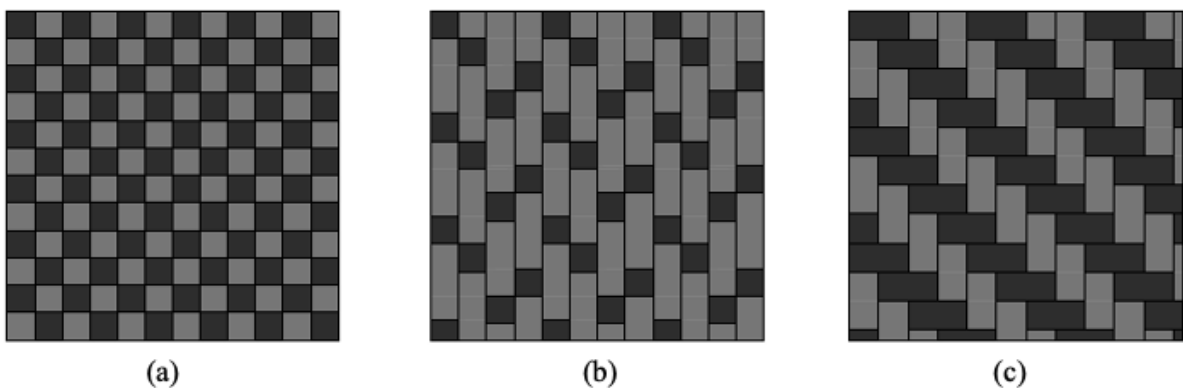
**Figure 2-9: Woven carbon fibers illustration, (a) plain weave, (b) 4HS harness satin weave, (c) 2x2 twill weave**

Figure 2-10 shows unidirectional fibers (non-woven). As seen, the fibers move in a unified and parallel direction and there are no gaps between fibers. Because there are no fibers that interrupt its pattern in any other direction, this allows for maximum longitudinal potential, which is greater than any woven fabric [34]. Since these fabrics are unidirectional, they are not ideal for applications that require anisotropic strength properties [34]. Therefore, in these kind of applications, woven fabrics would be preferred. Another drawback of unidirectional fibers are their low workability; they tend to easily fall apart during the layup process since there are no interlaced fibers to hold the longitudinal fibers together [35].
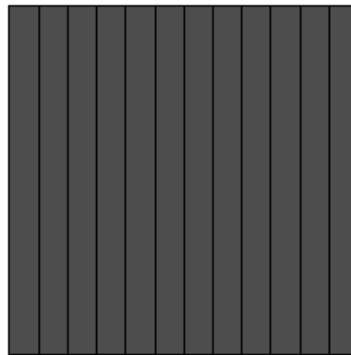


**Figure 2-10: Unidirectional carbon fiber illustration**

The use of carbon fibers in the form of fabric impregnated in epoxy resin increases the peak compressive load capacity of the material as more reinforcing layers and a higher fiber volume content is applied to the structure [8, 21]. The selected manufacturer of carbon fiber sheets and epoxy resin used in this research, Simpson Strong-Tie, recommends their Composite Strength System (CSS) fibers to be saturated with epoxy resin types A and B in a mixing proportion of 2A:1B [36].

It is important to note that the layup of these fibers in relation to the tube and to each other directly affects the performance of the material. On composite tubes with four layers of unidirectional epoxy-impregnated CFRP, sheets of orientation [0°/90°/0°/90°], as shown in Figure 2-11, are preferred as the energy absorption capability is increased compared to [90°/0°/90°/0°] as investigated by Abada et al. [16]. This notation corresponds to the angle of fibers in relation to the tube. Also, according to Yalçın et al. [21], CFRP reinforcement decreases the magnitude of the oscillation of the load-displacement curves of hollow

aluminum tubes, which has a more plateau-like behavior, which increases the efficiency of the system [26].
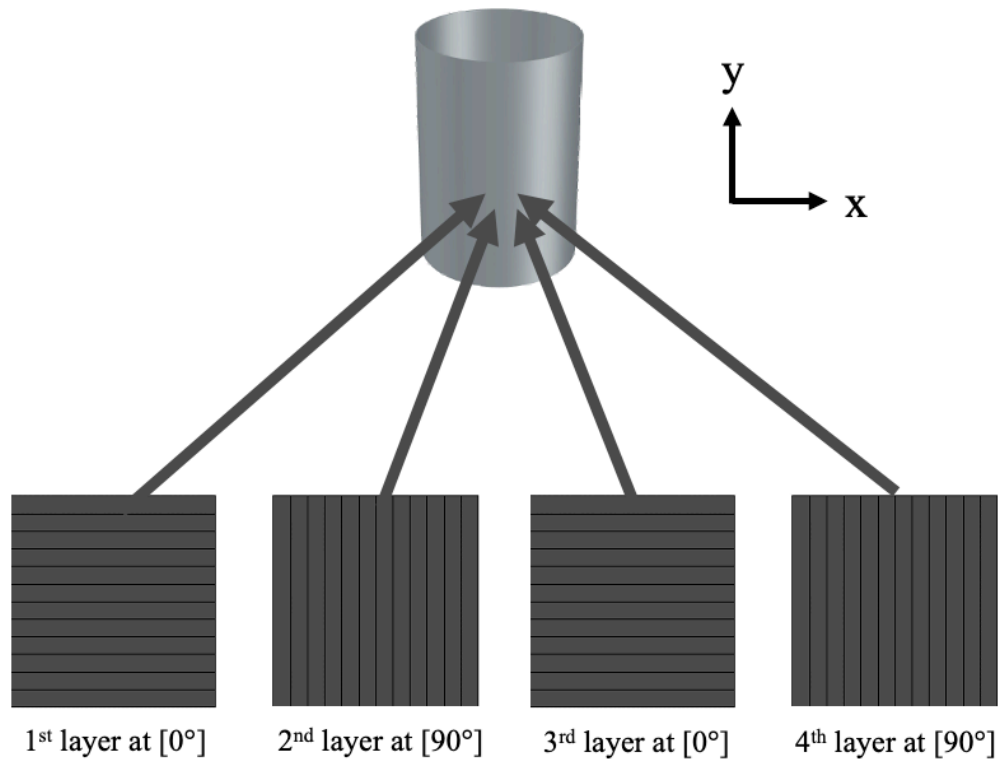


**Figure 2-11: Illustration of a [0°/90°/0°/90°] unidirectional CFRP layup**

## 2.4.3 Core Materials

Core materials, acting alternatively or in addition to FRP reinforcement, can be used to increase the energy absorption of structures. Because the development of these materials are relatively recent and they are constantly under improvement, these are the material components that engineers commonly have the least knowledge about [37]. These structures have a high strength-to-weight ratio and because of that, it is desired that these core materials have low densities, high shear strength, and stiffness perpendicular to the faces [37]. Honeycomb and cellular foams are common core materials that can be implemented to the specimen to increase its crashworthiness [26].

Although honeycomb cores are primarily known for their aerospace applications, cheaper honeycomb materials made of impregnated paper are also used in building applications [37]. These materials are manufactured in a wide range of cell size and shapes such as hexagonal, square, rectangular, and corrugated [37]. The most common honeycomb core materials are aluminum and impregnated glass or aramid fiber mats. Generally, cellular foams have lower stiffness and strength-to-weight ratio than honeycombs, but they have unique advantages [37]. Because these materials are solid on a macroscopic level, they require less labor to be manufactured and installed and, as a result, are in general less expensive than honeycombs. Most foams can be bonded to other materials and together by adhesives, which should be able to carry the same shear stress as the core [38], and are shapeable in almost any kind of form, allowing freedom in design [38]. In addition, they are non-corrosive, offer good thermal and sound insulation, and have very low water absorption [38]. Foams offer high stiffness and strength even with low density and can fully compressed with almost the same force before densification [21]. One of the first investigations of the crashworthiness of foam-filled tubular structures dates back to the early 1980s, which pointed out that these structures had a noticeable specific energy absorption increase when compared to hollow tubular structures [39]. Later, it was found that these materials offer superior properties for aluminum tubes rather than for steel tubes as investigated by Alia et al. [40].

During the manufacturing process of cellular foams, their cells can be either form an interconnected network (open-cell foam) or be sealed (closed-cell foam) [41]. Because the former has larger voids, open-cell foams are generally less expensive, softer and more flexible than closed-cell foams [42]. Air and moisture are unable to penetrate closed-cell foams, creating a denser material with much more rigidity and stability [42]. Because of these properties, closed-cell foams are much more appropriate to energy absorption cores, while open-cell foams are advantageous as insulating and soundproofing materials [42]. Some examples of foams that can be used as a filler material are polyurethane (PU), polystyrene (PS), polymethacrylimide (PMI), and polyvinyl chloride (PVC) foams [7, 37]. Each of these foams have benefits and preferred applications. Therefore, it is important to understand each of these.

*PU foam:* This material is produced predominantly in closed-cell rigid types in densities that range from 30 to 500 kg/m$^3$ [37]. The main advantages of PU foams are their low cost and very good insulation properties. Their application as energy absorbers is quite limited due to their lower mechanical properties when compared to other cellular cores [37].

*PS foam:* Similarly to PU foams, PS foams are predominantly produced in closed-cell rigid types and their densities range from 15 to 300 kg/m$^3$ [37]. Similarly to PU foams, PS foams have low cost and low mechanical properties, and are mainly used as insulation materials [37].

*PMI foam:* This material has very fine and closed cells; its densities range from 30 to 300 kg/m$^3$ [37]. In general, it has the best mechanical properties, but is also the most expensive cellular foam. Its temperature resistance is also outstanding and it often used in conjunction with epoxy prepregs in autoclave manufacturing [37].

*PVC foam*: Differently from PMI foams, PVC foams soften at very high temperatures are not commonly used at these conditions. This material is used in almost any application and exists in cross-linked and linear [43] forms with the former being less heat sensitive and commonly used as energy absorbers due to their higher mechanical properties and rigidity [37]. In fact, this is the most widely used foam [37] for this application. Also, it is important to note that lower density PVC foams have about 95% closed cells and almost entirely closed cells for higher densities [37]. Because this makes this material a very good energy absorber even at low densities, PVC foam was selected as the core material in this research and its literature will be further elaborated next.

### 2.4.3.1 PVC Foam Cores

Eksi et al. [26] experimentally investigated the behavior of plain and pre-formed aluminum tubes of 60 mm height, 1 mm wall thickness, and 50 mm outer diameter with 60 kg/m$^3$ density PVC foam core under axial quasi-static load of 60 mm/min rate. Yalçın et al. [27] examined the effect of radially graded PVC foam filling on crashworthiness of aluminum tubes. In addition, the influence of CFRP and PVC foam (80 kg/m$^3$ density) reinforcements on the energy absorption capability of composite aluminum tubes of 50 mm height, 1.25 mm wall thickness, and 58.5 mm diameter has been investigated [21] under quasi-static axial load of 60 mm/min. Through this research it was found that CFRP strengthening has a higher energy

absorption effectiveness than PVC foam cores. These supplemental materials acting together can greatly improve the crashworthiness of a specimen. This is because the PVC foam tends to increase the average crushing load by providing an inward wall support, while the CFRP mainly increases the peak force and supports the tube wall from outward movement [21]. Alia et al. [40] observed that foams do not significantly modify the response of the tube; they primarily act as a substrate to hold the tubes in place. Because of this, Alia et al. [40] noted that the density of the foam should be as low as possible.

PVC foam core sheets with multiple densities are offered in the market (from 30 kg/m$^3$ to 250 kg/m$^3$). Although it is expected that the absorbing performance increases with denser sheets, these may have different and more severe effects on failure mechanisms due to their increased weight. Also, it is important to note that the change in weight also affects the specific energy absorption of the tube. A few manufacturers lead the sandwich structure core market and Diab is known for their traditional Divinycell H foams, which are mainly used for energy absorption purposes. These foams are cross-linked with polyurea and PVC at almost equal parts forming an Inter Penetrating Network (IPN) [38] and are compatible with virtually all commonly used resin and manufacturing systems [44]. Divinycell H80 is a widely-used grade for this material that suits the objectives of this research and has very good mechanical properties with relatively low density (80 kg/m$^3$). Thus, it was the selected grade for this research.

# CHAPTER 3: EXPERIMENTAL PROGRAM

## 3.1 INTRODUCTION

An experimental investigation on the effect of foam adhesives on the energy absorption capability of aluminum tubes has not been done before. This will  be done by comparing the energy absorption quantities and failure modes of specimens with epoxied and non-epoxied foam-filled cores. In addition, an investigation on the influence of PVC foam core and CFRP reinforcements on the crashworthiness of tall composite aluminum tubes through quasi-static axial loading has not been done and is needed. By performing this investigation and comparing it with an analysis of tubes different specimen lengths, is possible to study the efficiency of these reinforcements on tubes of different L/D ratios.

The details of the experimental program conducted at the University of Idaho are discussed and reported in this chapter. The tests comprised of circular aluminum tubes of 1.6 mm wall thickness, 60 mm inner diameter, and different heights: 40 mm, 80 mm and 120 mm. All specimens were tested under quasi-static axial compression load. Tall specimens (of 120 mm) had varying combinations of CFRP and PVC foam reinforcements while shorter specimens (of 80 mm and 40 mm) were assembled with both CFRP and PVC foam reinforcements combined.

## 3.2 TEST OBJECTIVES

The objectives of the experimental program were to:

1.  Investigate the effect of epoxy as an adhesive to bond the tube with the PVC foam on the energy absorption capability of the tubes.
2.  Investigate the behavior of TW circular aluminum tubes under quasi-static axial loading.
3.  Study the influence of CFRP and PVC foam reinforcements on the crashworthiness of these tubes.
4.  Understand and investigate the influence of these reinforcements on the crashworthiness of specimens of different L/D ratios.

## 3.3 MATERIAL PROPERTIES

### 3.3.1 Aluminum Tubes

Round aluminum alloy tubes of 6061-T6 were used for this research. These come as tall tubes of 1.6 mm (1/16 in.) wall thickness and 60 mm inner diameter. Table 3-1 shows the physical and mechanical properties of the AA6061-T6 tubes.

**Table 3-1: AA6061-T6 properties**

| Parameter | Value | Unit |
|---|---|---|
| Density | 2.70 | $g/cm^3$ |
| Poisson's ratio | 0.33 | - |
| Modulus of elasticity | 68.9 | GPa |
| Tensile strength, ultimate | 310 | MPa |
| Tensile strength, yield | 276 | MPa |
| Elongation (1/16 in.) | 12 | % |
| Hardness, Brinell | 95 | % |
| Shear modulus | 26 | GPa |
| Shear strength | 207 | MPa |
| Fatigue endurance limit | 97 | MPa |

### 3.3.2 CFRP

Unidirectional Simpson Strong-Tie carbon fiber sheets and manufacturer epoxy resin types A and B were donated by the manufacturer. Properties of the CFRP after proper surface preparation, mixing, installation, and curing are seen in Table 3-2.

**Table 3-2: CFRP properties [16]**

| Parameter | Value | Unit |
|---|---|---|
| Density | 1.45 | kg/m³ |
| Modulus of elasticity X | 121000 | MPa |
| Modulus of elasticity Y | 6800 | MPa |
| Modulus of elasticity Z | 6800 | MPa |
| Poisson's ratio XY | 0.27 | - |
| Poisson's ratio YZ | 0.40 | - |
| Poisson's ratio XZ | 0.27 | - |
| Shear modulus XY | 4700 | MPa |
| Shear modulus YZ | 3100 | MPa |
| Shear modulus XZ | 4700 | MPa |
| Axial tensile strength | 2245.3 | MPa |
| Axial compressive strength | 1924.1 | MPa |
| Transverse tensile strength | 55.6 | MPa |
| Transverse compressive strength | 198.5 | MPa |

Properties of the cured epoxy are shown in Table 3-3.

**Table 3-3: Epoxy properties [36]**

| Parameter | Value | Unit |
|---|---|---|
| Density | 1.15 | kg/L |
| Tensile strength | 36 | MPa |
| Tensile modulus | 2200 | MPa |
| Elongation at break | 1.73% | - |
| Flexural strength | 63 | MPa |
| Flexural modulus | 3660 | MPa |
| Compressive strength | 109 | MPa |
| Compressive modulus | 2990 | MPa |

### 3.3.3 PVC Foam

Closed-cell Divinycell H80 foam sheets of ½-inch thickness were kindly donated by Diab Group. Properties of this PVC foam are seen in Table 3-4.

**Table 3-4: Divinycell H80 PVC foam properties**

| Parameter | | Value | Unit |
|---|---|---|---|
| Density | Nominal | 80 | kg/m$^3$ |
| Poisson's ratio | - | 0.40 | - |
| Compressive strength[1] | Nominal | 1.40 | MPa |
| | Minimum | 1.15 | MPa |
| Compressive modulus[1] | Nominal | 90 | MPa |
| | Minimum | 80 | MPa |
| Tensile strength[1] | Nominal | 2.5 | MPa |
| | Minimum | 2.2 | MPa |
| Tensile modulus[1] | Nominal | 95 | MPa |
| | Minimum | 85 | MPa |
| Shear strength | Nominal | 1.15 | MPa |
| | Minimum | 0.95 | MPa |
| Shear modulus | Nominal | 27 | MPa |
| | Minimum | 23 | MPa |
| Shear strain | Nominal | 30 | % |

[1]Properties measured perpendicular to the plane

## 3.4 PREPARATION OF SPECIMENS

Using the circular aluminum tubes, a total of seven different sample configurations were designed and assembled at the University of Idaho Buchanan Engineering Lab. At least two specimens for each reinforced configuration were prepared to provide validation of their properties. Table 3-5 summarizes the prepared specimens and describes their assigned naming, configuration, and the materials used. Each of the specimen preparation steps will be elaborated in this section. Figure 3-1 and Figure 3-2 show each of the prepared specimen configurations.
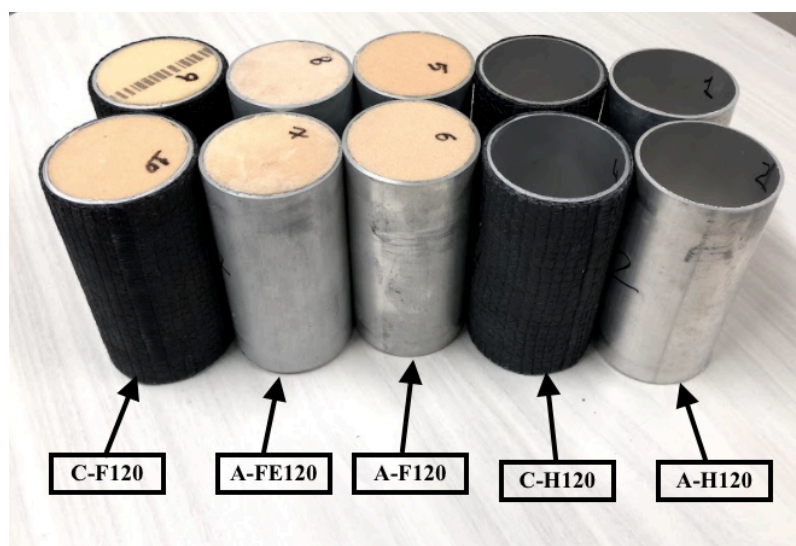


**Figure 3-1: Specimen configurations of 120 mm in length**
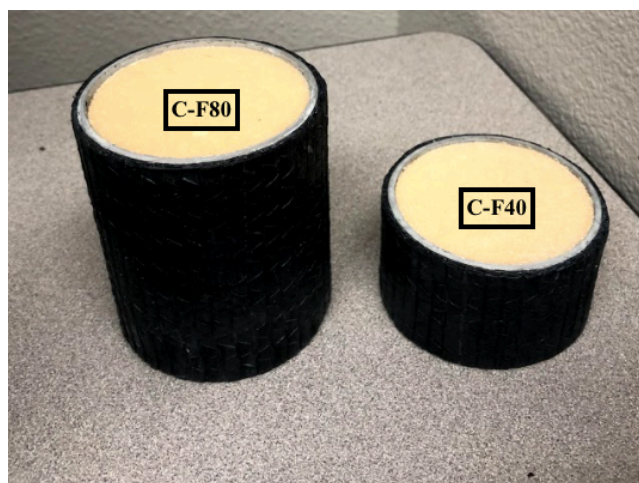


**Figure 3-2: Specimen configurations of 80 mm and 40 mm in length**

**Table 3-5: Summary and description of prepared specimens**

| Specimen | Configuration | Average Mass (g) | Length (mm) | Materials |
|---|---|---|---|---|
| Hollow tube (A-H120) | | 106.2 | 120 | AA6061-T6 |
| Composite hollow tube (C-H120) | | 153.8 | 120 | AA6061-T6, CFRP |
| Foam-filled tube (A-F120) | | 132.1 | 120 | AA6061-T6, PVC foam |
| Tube with epoxied foam-filled core (A-FE120) | | 144.0 | 120 | AA6061-T6, PVC foam |
| Composite foam-filled tube (C-F120) | | 178.8 | 120 | AA6061-T6, CFRP, PVC foam |
| Composite foam-filled tube (C-F80) | | 119.1 | 80 | AA6061-T6, CFRP, PVC foam |
| Composite foam-filled tube (C-F40) | | 59.4 | 40 | AA6061-T6, CFRP, PVC foam |

### 3.4.1 Aluminum Tubes

Tubes of 40 mm, 80 mm, and 120 mm in length were measured and the cut using a heavy duty tube cutter as seen in Figure 3-3. These tubes were used for the preparation of the specimens seen in Table 3-5.



Figure 3-3: Cutting equipment for aluminum tubes

### 3.4.2 CFRP Reinforcement

The desired widths and lengths of carbon fiber sheets were cut from the sheet, seen in Figure 3-4. Epoxy of types A and B were mixed in a 2A:1B ratio, as recommended by the manufacturer, until a homogenous solution was achieved, and used to bond the carbon fiber sheet with the aluminum tube. Tensioning was applied during this wrapping procedure to ensure no trapped air and no unwanted additional thickness. The total thickness was 1.6 mm with a [0°/90°/0°/90°] layup. As previously mentioned, this orientation nomenclature corresponds to the fiber direction with respect to the applied surface.

**Figure 3-4: Carbon fiber unidirectional sheet**

After the specimens went through the manufacturer's recommended curing process, the ends of the CFRP reinforcement were trimmed to ensure no uneven ends, which could cause eccentricity during testing. Figure 3-5 shows some of the CFRP reinforced tubes during the curing process. These reinforced tubes were used for the preparation of the C-H120 and all C-F specimens (C-Fs).



**Figure 3-5: CFRP reinforced samples during curing process**

### 3.4.3 PVC Foam

63 mm x 63 mm square foams were measured and cut from the 1.22 m x 1.22 m (4 ft x 4 ft) square PVC foam sheet using a razor knife as seen in Figure 3-6.
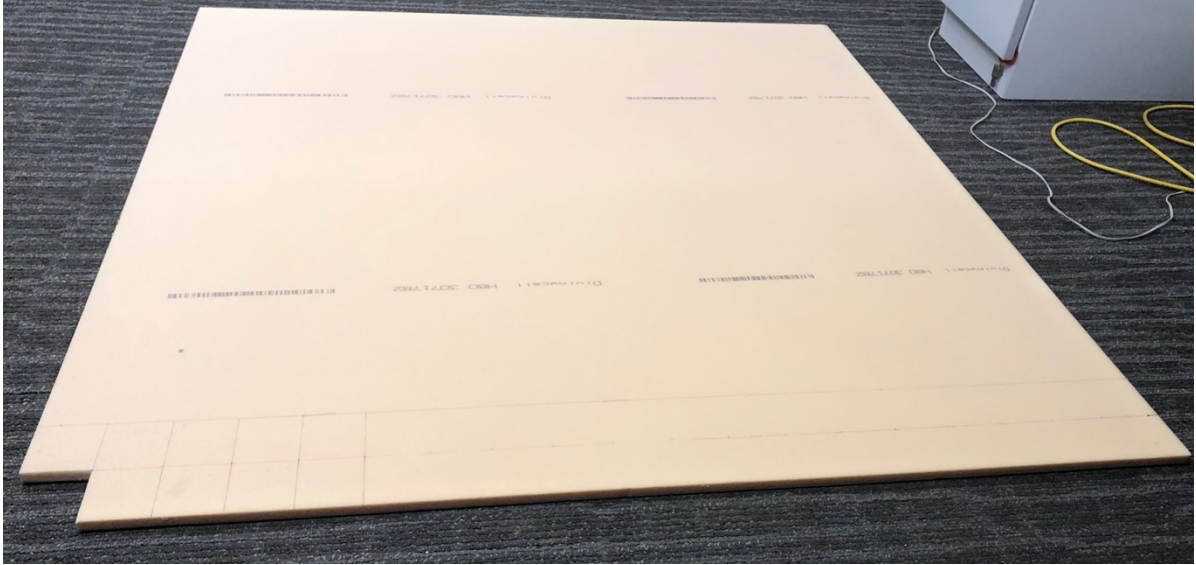


**Figure 3-6: PVC foam sheet with measured cutting sections**

Next, these squares were trimmed using the same tool to tightly fit the 60 mm tube's inner diameter as seen in Figure 3-7.



**Figure 3-7: PVC foam cut into circles and squares**

The same epoxy materials and preparation used for the CFRP reinforcement were used for the preparation of epoxy foam-filled specimens (A-FE120). The adhesive was applied to both the interior surface of the tubes and the sides of the PVC foam circular layers in such a manner that the epoxy stays in place when the foam layers are tightly placed in the tube. It is important to note that the adhesive was not used between the layers since under axial loading, it is not expected that this would improve the specimen performance and it would decrease the specific energy absorption capability of the structure as its weight is increased. After, foam layers were stacked inside the tube and subjected to the curing process.

For the preparation of non-epoxied foam-filled specimens (A-F120 and C-Fs), the layers were stacked inside the tube and a small amount of adhesive was used to bond only the top and bottom foam layers to the aluminum tube. Although it was expected that the foam would not slide from the tube, it was necessary to secure these layers of foam for storing and transporting purposes. Finally, the foam was trimmed to ensure a flat surface at the extremities of the tube. Figure 3-8 shows C-F80 and C-F40 tubes during curing process.



**Figure 3-8: C-F80 and C-F40 tubes during curing**

## 3.5 TESTING PROCEDURES

To investigate the crashworthiness of the specimens, quasi-static axial compression tests were performed at the University of Idaho McClure Hall Materials Testing Lab using a material test system (MTS-810) machine with computer control and data acquisition system as seen in Figure 3-9. The specimen was centered with the 155.6 mm diameter (6 1/8") machine plates and compressed at a 8 mm/min constant loading rate until a crushing displacement equal to 50% of the initial specimen length was achieved. The test was limited to this maximum displacement to avoid the excessive loading of the machine and provide consistency between specimens. Load and displacement data was automatically generated and recorded by the data acquisition system. Using this data, load-displacement curves were plotted and crashworthiness quantities could be calculated.
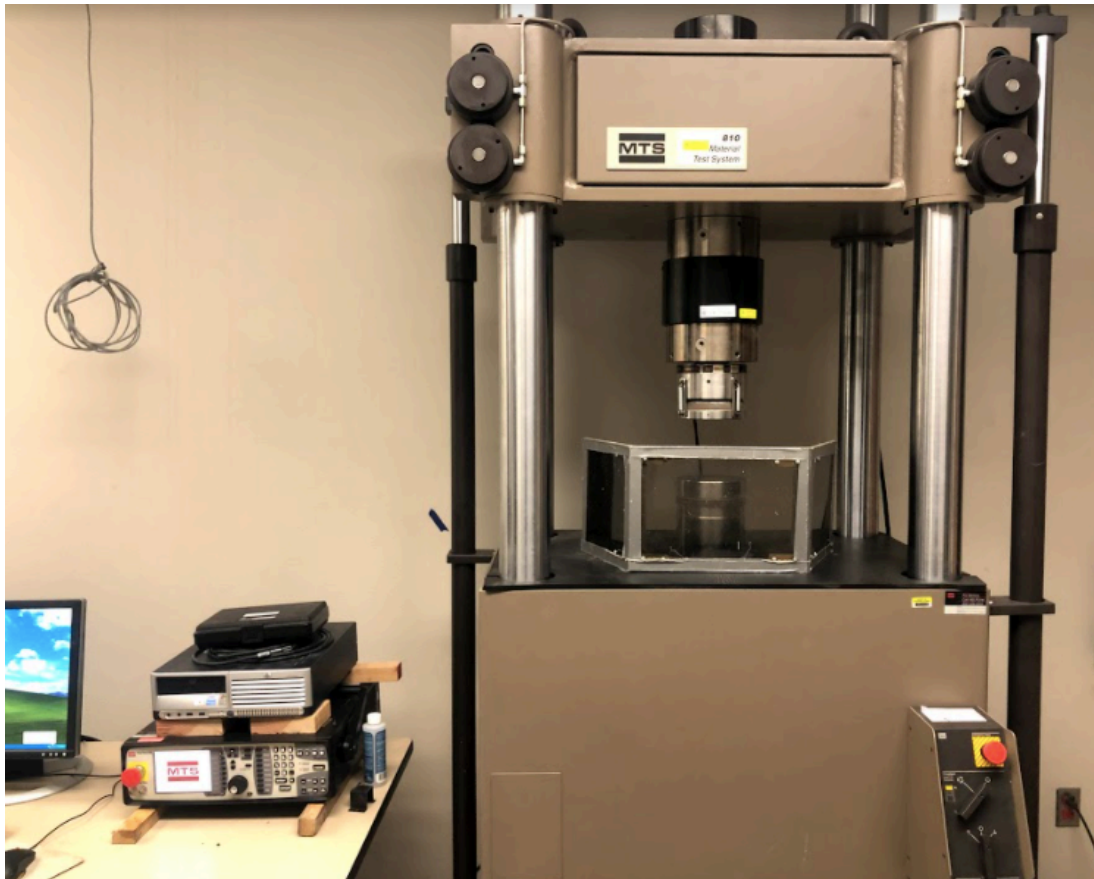


**Figure 3-9: MTS-810 machine used for quasi-static tests**

# CHAPTER 4: RESULTS AND DISCUSSIONS

## 4.1 INTRODUCTION

This chapter discusses the outcomes of the experimental program presented in Chapter 3. The main objective of the experiment is to investigate the crashworthiness behavior of the prepared specimens. This investigation consists of:

1. Validating each specimen configuration by observing the crushing behavior and comparing calculated crashworthiness quantities from the acquired testing data for the prepared specimens for each configuration; small differences between these calculated quantities validate each specimen configuration.

2. Analyzing the crashworthiness of different specimen configurations by observing the failure modes and comparing calculated quantities; configurations with more predictable behavior and superior quantities have better crashworthiness performance.

## 4.2 PERFORMANCE UNDER QUASI-STATIC AXIAL LOADING

### 4.2.1 Aluminum Tubes (A-H120)

To determine the crashworthiness quantities and observe the failure mode of unreinforced aluminum tubes, a specimen with 120 mm in length was tested under quasi-static axial load. This configuration served as the "control" specimen, which allows for the determination of the effects of the reinforcements on crashworthiness. The load-displacement curve for the specimen is shown in Figure 4-1.
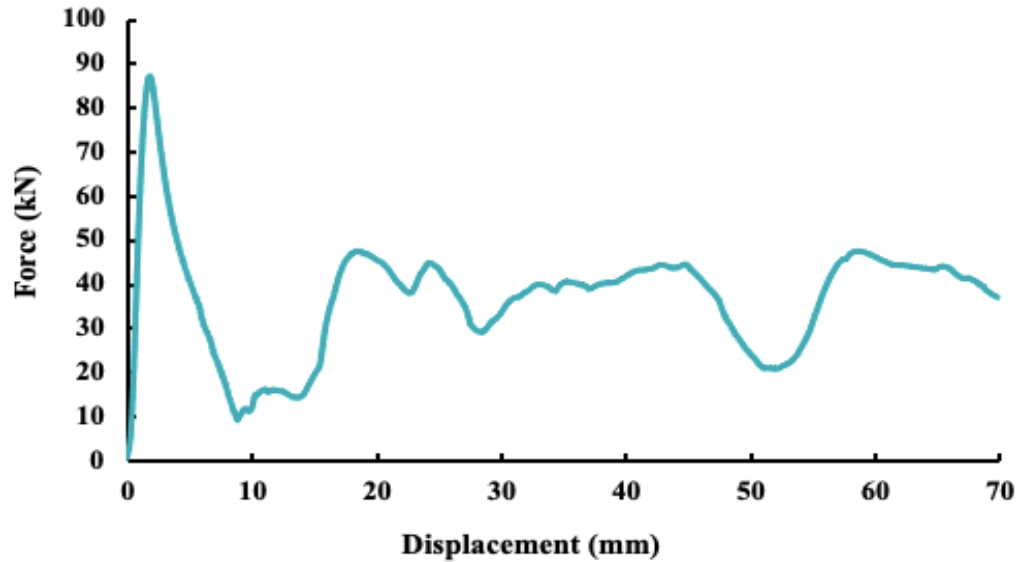
**Figure 4-1: A-H120 load-displacement plot**

Since this configuration consists of only the aluminum material, its behavior is very consistent. To verify this, the calculated values have been compared to Abada et al. [16], which tested aluminum tubes with the same properties and with the same geometry. His specimens were tested until a 70 mm crushing, the same as performed for the tested specimen in this study. The calculated crashworthiness quantities are seen in Table 4-1.

**Table 4-1: A-H120 calculated quantities and discrepancy**

| Specimen | Mass (g) | $P_{max}$ (kN) | $P_{avg}$ (kN) | $E_c$ (kJ) | EA (kJ) | SEA (J/g) | CFE |
|---|---|---|---|---|---|---|---|
| 1 | 106.2 | 87.3 | 36.9 | 2.52 | 2.60 | 24.5 | 42.3% |
| 2* | 106.0 | 89.4 | 36.0 | ** | 2.39 | 23.6 | 41.0% |
| Discrepancy | 0.2% | 2.4% | 2.5% | - | 3.8% | 3.8% | 1.3% |

*From Abada et al.

**Data not provided

As seen, the various quantities are in very good agreement. Although the specimen tested by Abada et al. had a higher peak force, the specimen tested for this study had superior quantities during the post-crushing zone. Table 4-1 also shows the discrepancy in each of the crashworthiness quantities between the specimens, in percent. It is confirmed that the

differences were consistently small between specimens and the discrepancy between all quantities were smaller than 4%.

As seen in Figure 4-2, as expected for aluminum tubes without core reinforcement, wall deformation was observed on the dynamic plate side of the tube as it was axially displaced. The deformed tube is also shown in the figure which clearly shows the diamond mode failure mechanism. It is worth noting that each high and low peak in the load-displacement plot was directly related to the inward and outward wall movement, which formed folds in diamond shape, as seen in the figure below. Through observing the failure mode and observing the load-displacement plots, it is concluded that these specimens failed progressively.
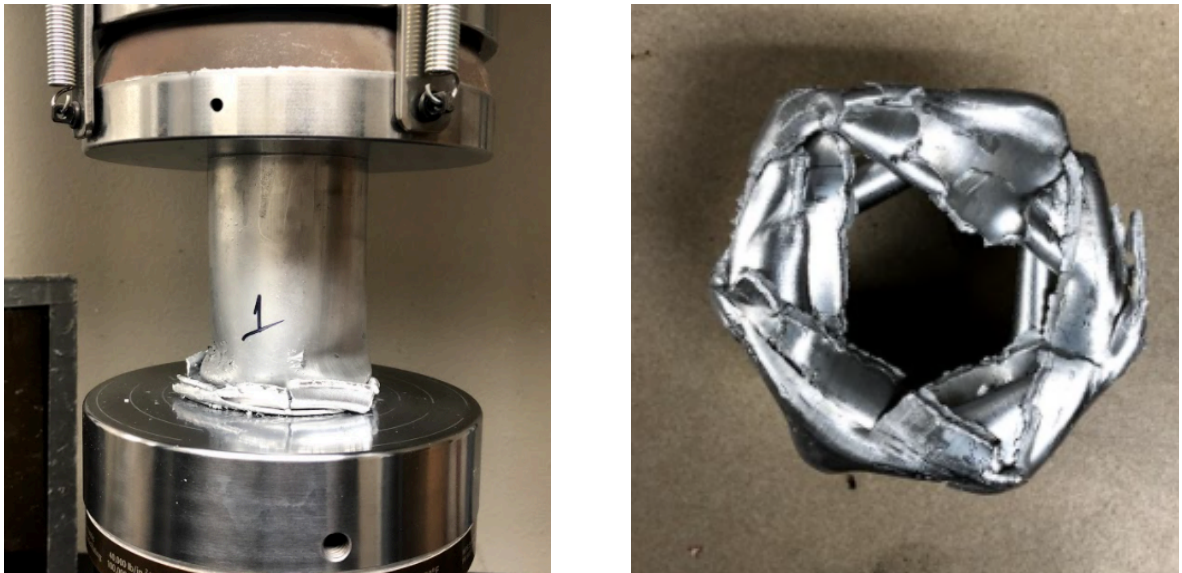
Figure 4-2: A-H120 crushing behavior

## 4.2.2 Aluminum Tubes with CFRP Reinforcement (C-H120)

Three hollow CFRP composite specimens with the same tube geometry as the A-H120 were tested to determine the effects of CFRP reinforcement on the crashworthiness of aluminum tubes. The load-displacement history for each of the specimens generated from the quasi-static axial tests is seen in Figure 4-3.
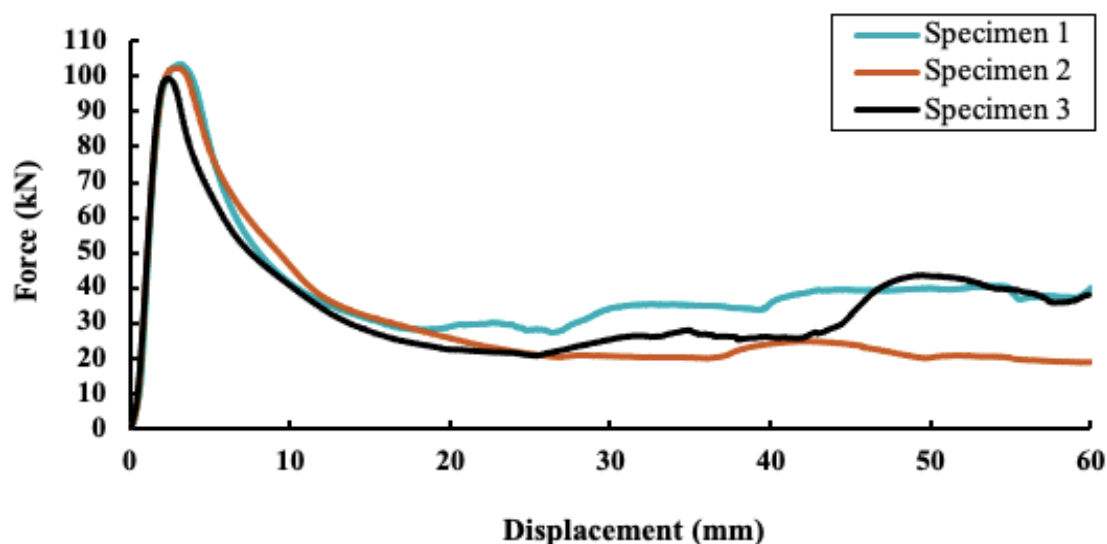
**Figure 4-3: C-H120 load-displacement plots**

From the plots, it is observed that the specimens have low forces in the post-crushing zone, generating a lower plateau. From quantities calculated from those plots, shown in Table 4-2, and the crushing behaviors, it is possible to conclude that these specimens failed catastrophically.

Table 4-2: C-H120 calculated quantities

| Specimen | Mass (g) | $P_{max}$ (kN) | $P_{avg}$ (kN) | $E_c$ (kJ) | EA (kJ) | SEA (J/g) | CFE |
|----------|----------|----------------|----------------|------------|---------|-----------|-----|
| 1 | 154.3 | 103.3 | 38.6 | 2.19 | 2.39 | 15.5 | 37.3% |
| 2 | 153.7 | 102.4 | 31.9 | 1.81 | 1.87 | 12.2 | 31.2% |
| 3 | 153.4 | 99.6 | 34.5 | 1.99 | 2.11 | 13.8 | 34.6% |

As seen in Figure 4-4, significant wall buckling occurred prior to the catastrophic failure, still at a low crushing displacement. Sudden failure occurred with greater axial displacement. This wall buckling may have been facilitated by small inconsistencies in the specimen preparation or during testing. As the CFRP adds considerable weight to the exterior of the tube wall and core reinforcement was not provided, this configuration had a more unpredictable behavior

and is more prone to wall buckling. Also, because the CFRP reinforcement restrains the tube wall from outward movement and no core support is provided, it displaced inwards.
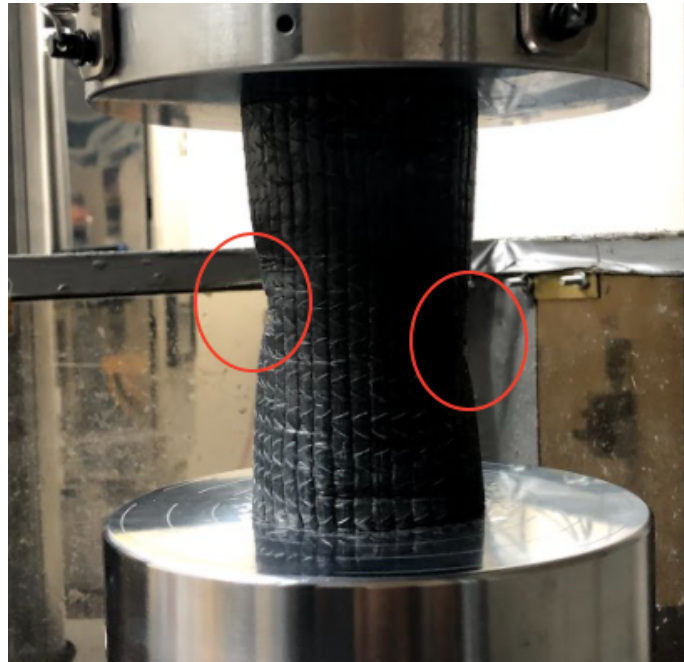


**Figure 4-4: C-H120 catastrophic wall buckling**

Figure 4-5 presents the observed post-testing deformed specimen. As seen, the wall buckling caused some eccentricity to the load with respect to the tube's wall, which deformed in a much more inefficient form. In addition, some minimal CFRP splaying was observed at the extremity of the tube.
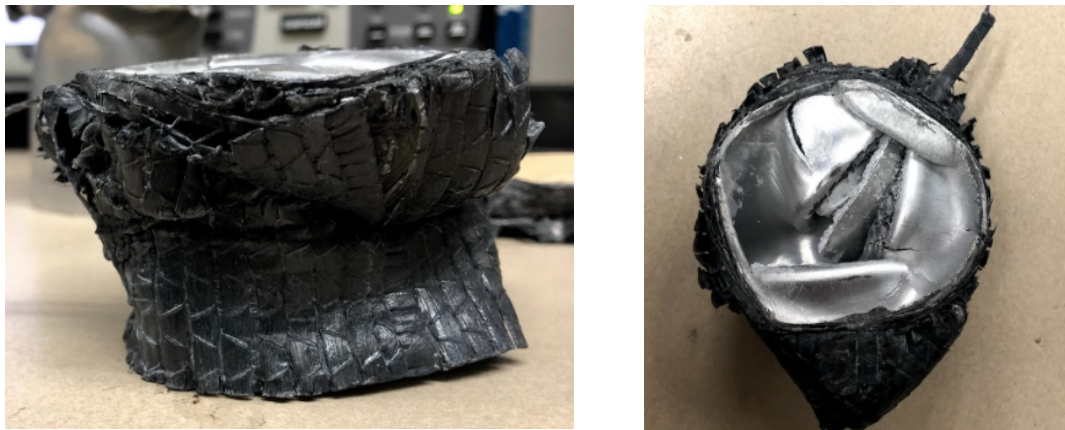


**Figure 4-5: C-H120 specimens after testing**

## 4.2.3 PVC Foam-Filled Aluminum Tubes (A-F120 and A-FE120)

To investigate the effect of foam adhesives on the crashworthiness of aluminum tubes, foam-filled specimens were tested. These tubes had 120 mm in length, 60 mm in inner diameter, and 1.6 mm in wall thickness and were tested with and without epoxy adhesion between the tube's wall and the foam material.

### 4.2.3.1 Non-Epoxied Foam Core (A-F120)

Two specimens with the same configuration were tested to validate this specimen configuration. Figure 4-6 shows the load-displacement plots generated from the quasi-static axial compression tests.
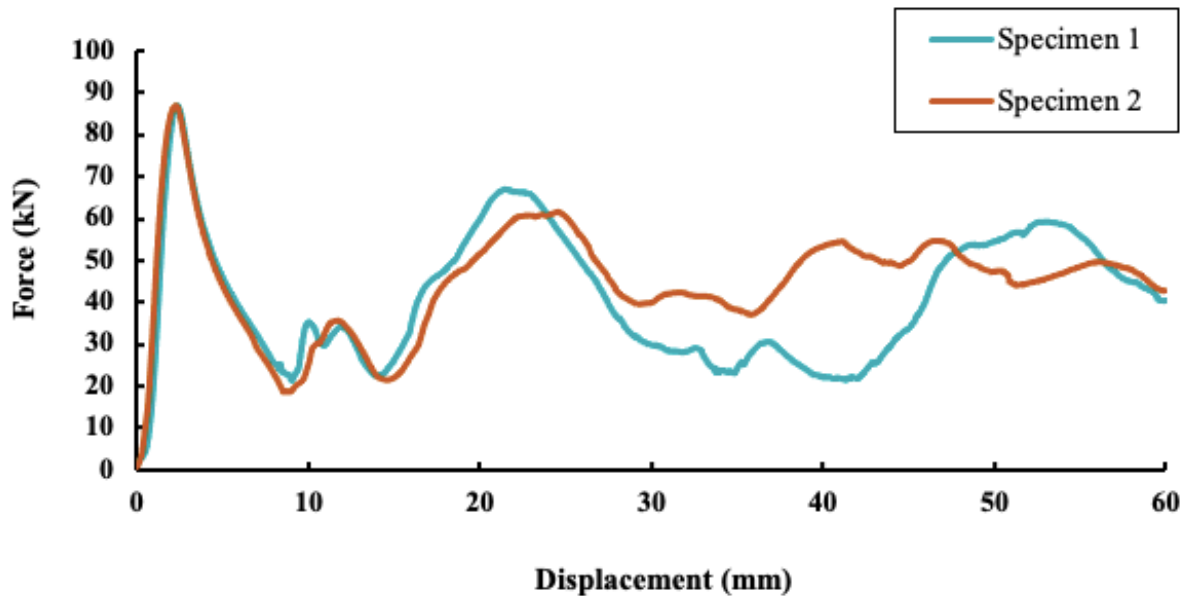


**Figure 4-6: A-F120 load-displacement plots**

As seen, both specimens behaved very similarly until the crushing displacement approached 25% the original specimen height. After a 30-mm displacement was achieved, different behaviors were observed and might have happened due to inconsistencies on the aluminum material. However, assessing the calculated crashworthiness quantities presented in Table 4-3, it is possible to notice consistency between the specimens.

**Table 4-3: A-F120 calculated quantities and discrepancy**

| Specimen | Mass (g) | $P_{max}$ (kN) | $P_{avg}$ (kN) | $E_c$ (kJ) | EA (kJ) | SEA (J/g) | CFE |
|----------|----------|-----------|-----------|---------|---------|-----------|-------|
| 1 | 131.5 | 87.1 | 41.2 | 2.38 | 2.47 | 18.8 | 47.3% |
| 2 | 132.6 | 87.0 | 44.8 | 2.58 | 2.69 | 20.3 | 51.4% |
| Discrepancy | 0.8% | 0.1% | 8.6% | 8.6% | 8.9% | 8.0% | 4.1% |

As seen, the difference in peak load between the specimens is 0.1%, while the average crushing force is about 3.5 kN greater for the second specimen. Also, it is important to notice a difference of about 1 gram in mass between the two tubes was observed, which confirms a slight inconsistency on the specimen preparation. Table 4-3 also shows the discrepancy in each of the crashworthiness quantities between the specimens, in percent.

As seen in Figure 4-7, a folding formation was observed near the dynamic plate at failure. These specimens did not suffer any inward wall displacement, which was prevented by the foam reinforcement. As seen from the top view, after testing, the foam did not remain connected to the tube's wall as enough adhesive was not provided to maintain the bond throughout the testing.
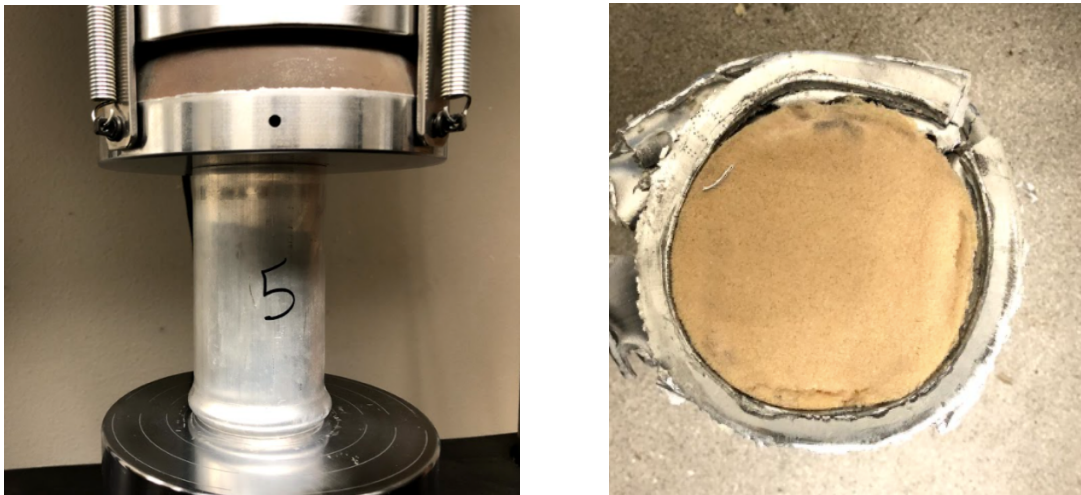


**Figure 4-7: A-F120 crushing behavior**

*4.2.3.2 Epoxied Foam Core (A-FE120)*

Two specimens were tested to validate this specimen configuration. The load-displacement plot for each of the specimens was generated from the quasi-static axial compression tests as shown in Figure 4-8.
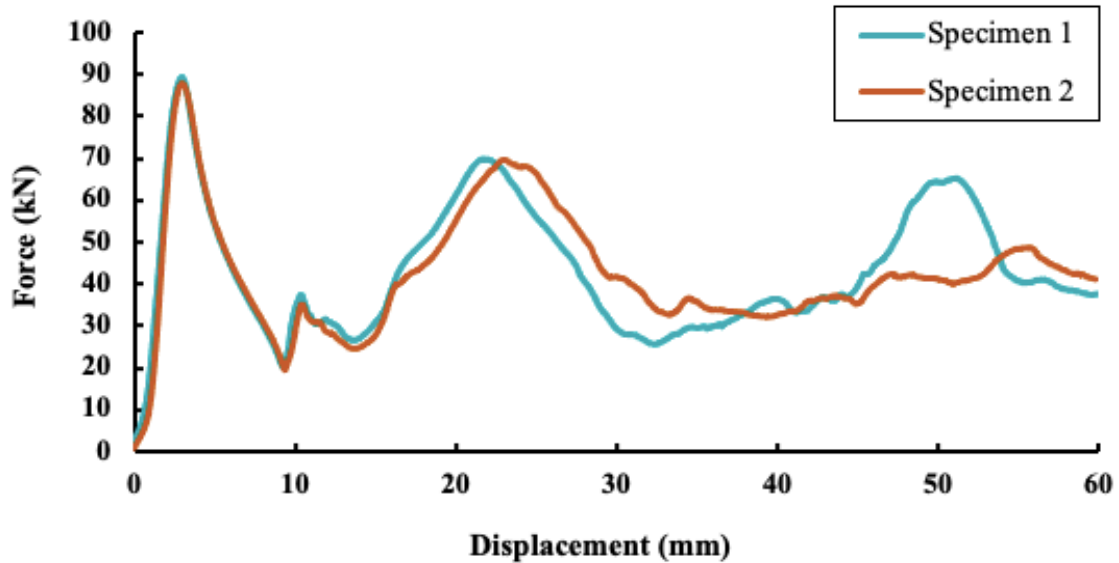


**Figure 4-8: A-FE120 load-displacement plots**

Similar to the A-F120 specimens, both specimens had the same behavior until the crushing displacement approached 25% the original tube length. After this point, the specimen behaviors differed, but remained at a similar average load. The calculated crashworthiness quantities for each specimen are shown in Table 4-4.

Table 4-4: A-FE120 calculated quantities discrepancy

| Specimen | Mass (g) | $P_{max}$ (kN) | $P_{avg}$ (kN) | $E_c$ (kJ) | EA (kJ) | SEA (J/g) | CFE |
|---|---|---|---|---|---|---|---|
| 1 | 143.2 | 89.5 | 43.3 | 2.47 | 2.60 | 18.2 | 48.4% |
| 2 | 144.7 | 88.1 | 40.9 | 2.33 | 2.56 | 17.7 | 46.4% |
| Discrepancy | 1.0% | 1.6% | 5.6% | 5.7% | 1.5% | 2.6% | 2.0% |

Both specimens yielded very similar values, for the quantities which validates the data for this configuration. The peak load differed by 1.6%, while the first specimen demonstrated an

average crushing load of 3 kN lower than the second specimen. Similarly to the previous specimens, there is a slight difference of 1.5 gram in mass between the two tubes, which confirms a small inconsistency on the specimen preparation. Table 4-4 also shows the discrepancy in each of the crashworthiness quantities, which ranged between 1% and 5.7%.

As seen in Figure 4-9, similar to the A-F120 configuration, at the peak load, a folding was observed near the dynamic plate. These specimens also did not suffer any inward movement of the tube wall, prevented by the foam reinforcement. The figure also shows the deformed tube after testing. Although this configuration yielded a very similar crushed shape, the epoxy caused the external foam layer to crack near the edge due to the folding at the peak load as the foam remained bonded to the tube wall. This confirms that the epoxy is stronger than the foam. However, throughout other locations along the tube length, the epoxy failed and outward wall movements were observed, which is related to the peaks on the load-displacement plots.



**Figure 4-9: A-FE120 crushing behavior**

**4.2.4 PVC Foam-Filled Aluminum Tubes with CFRP Reinforcement (C-Fs)**

The following specimens with constant inner diameter of 60 mm and varying lengths were tested under quasi-static axial load:

- C-F120: 120 mm in length and L/D = 2.00
- C-F80: 80 mm in length and L/D = 1.33
- C-F40: 40 mm in length and L/D = 0.67

This was done to investigate the effects of length-to-diameter ratio (L/D) on crashworthiness of foam-filled CFRP composite aluminum tubes.

*4.2.4.1 C-F120*

Two specimens of 120 mm in length were tested under quasi-static load to validate this configuration. Their generated load-displacement plots are seen in Figure 4-10.



**Figure 4-10: C-F120 load-displacement plots**

As seen, the specimens have very similar behavior throughout the testing, with a plateau-like behavior in the post-crushing zone. Crashworthiness quantities were calculated from the load-displacement plots for each of the specimens, as presented in Table 4-5.

**Table 4-5: C-F120 calculated quantities and discrepancy**

| Specimen | Mass (g) | $P_{max}$ (kN) | $P_{avg}$ (kN) | $E_c$ (kJ) | EA (kJ) | SEA (J/g) | CFE |
|---|---|---|---|---|---|---|---|
| 1 | 179.2 | 102.8 | 48.2 | 2.73 | 2.97 | 16.6 | 46.9% |
| 2 | 178.4 | 106.6 | 49.6 | 2.83 | 2.98 | 16.7 | 46.5% |
| Discrepancy | 0.4% | 3.7% | 2.8% | 3.9% | 0.5% | 0.9% | 0.4% |

Comparing these quantities, shows that the specimens produced very similar behaviors. Table 4-5 also presents the discrepancy between each of the presented quantities, which ranges from 0.4% and 3.9%.

Figure 4-11 shows some inward wall movement which was restrained by the foam. The CFRP, on the other hand, restrained the tube wall from failure due to outward movement. These supports are essential for a progressive deformation at a higher plateau, which can be noticed in the load-displacement curves. If these supports were not provided, any wall deformation could promptly lead to catastrophic failure. After testing, it was also possible to observe a minimal CFRP splaying at the extremity of the tube, as seen in the figure.



**Figure 4-11: C-F120 crushing behavior**

## 4.2.4.2 C-F80

Two specimens of 80 mm in length were tested under quasi-static axial load to validate this configuration. The generated load-displacement plots are seen in Figure 4-12.



**Figure 4-12: C-F80 load-displacement plots**

The specimens have nearly identical curves until a 10 mm crushing is achieved. After that, during the plateau, the curves show slightly different behaviors, but at similar forces. The calculated quantities are seen in Table 4-6.

Table 4-6: C-F80 calculated quantities and discrepancy

| Specimen | Mass (g) | $P_{max}$ (kN) | $P_{avg}$ (kN) | $E_c$ (kJ) | EA (kJ) | SEA (J/g) | CFE |
|----------|----------|----------------|----------------|------------|---------|-----------|-----|
| 1 | 118.8 | 105.6 | 48.2 | 1.78 | 2.00 | 16.8 | 45.6% |
| 2 | 119.4 | 106.8 | 50.5 | 1.85 | 2.08 | 17.4 | 47.2% |
| Discrepancy | 0.5% | 1.2% | 4.8% | 4.4% | 4.2% | 3.6% | 1.6% |

The specimens have similar values for all quantities, which confirms consistency between them. As also seen in Table 4-6, the greatest discrepancy is of 4.8%, or of about 2 kN, for the average crushing load.

Figure 4-13 presents the crushing behavior for this configuration. A more considerable CFRP splaying was observed, and similar to the C-F120, some wall deformation occurred, which was resisted by the foam and by the CFRP. Due to these supports, a progressive failure was observed.



**Figure 4-13: C-F80 crushing behavior**

### 4.2.4.3 C-F40

Two specimens of 40 mm in length were tested under quasi-static axial load to validate this configuration. Their load-displacement plots are presented in Figure 4-14.
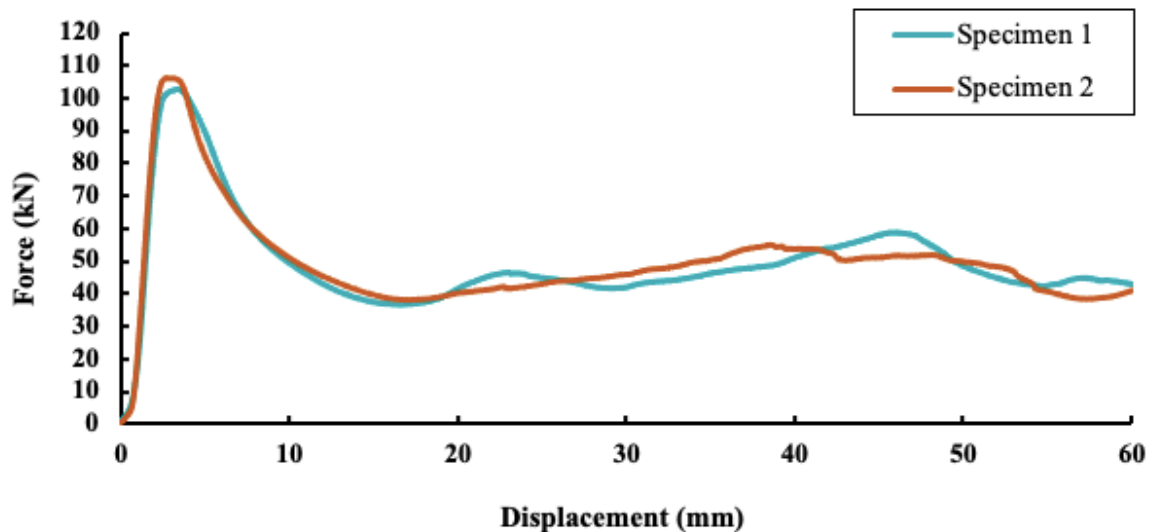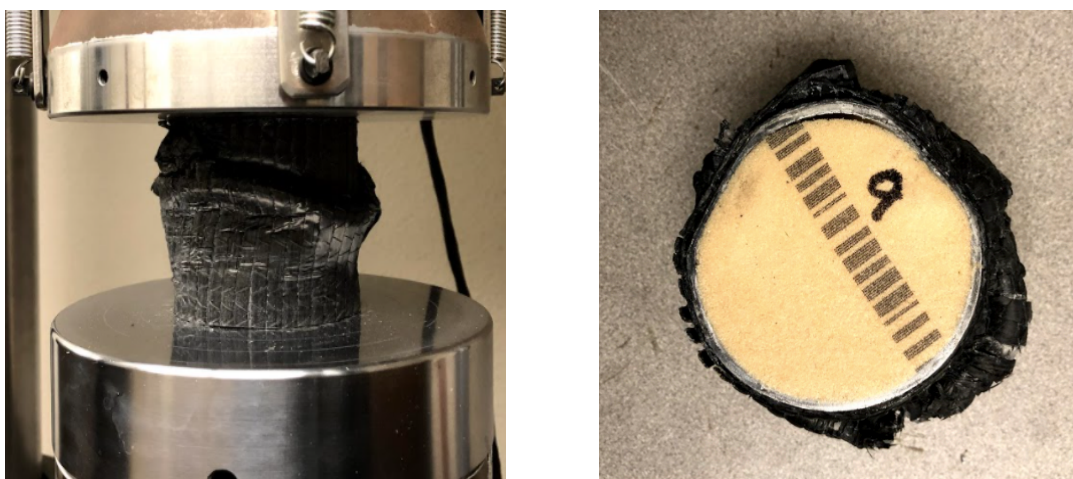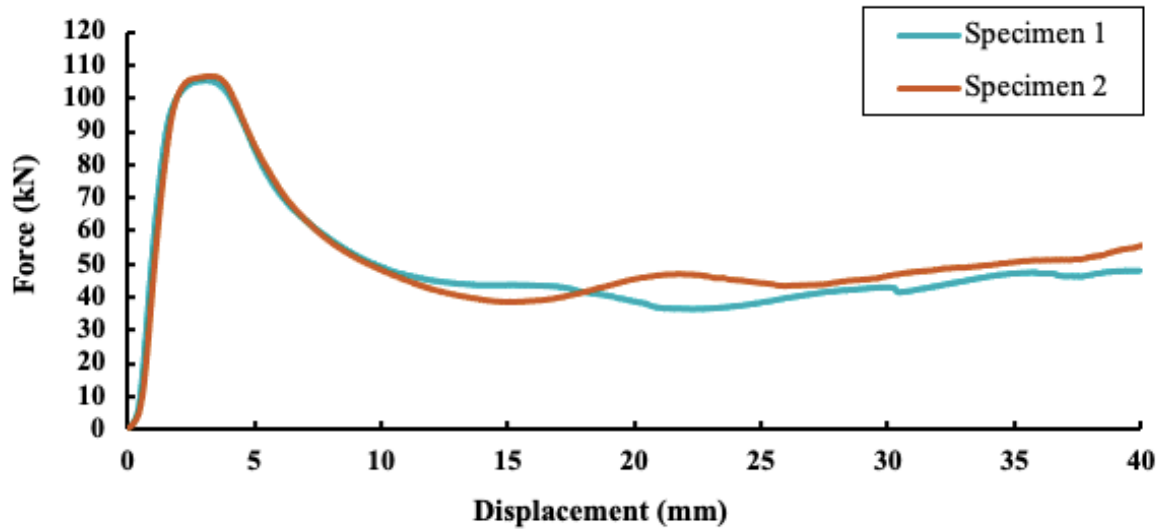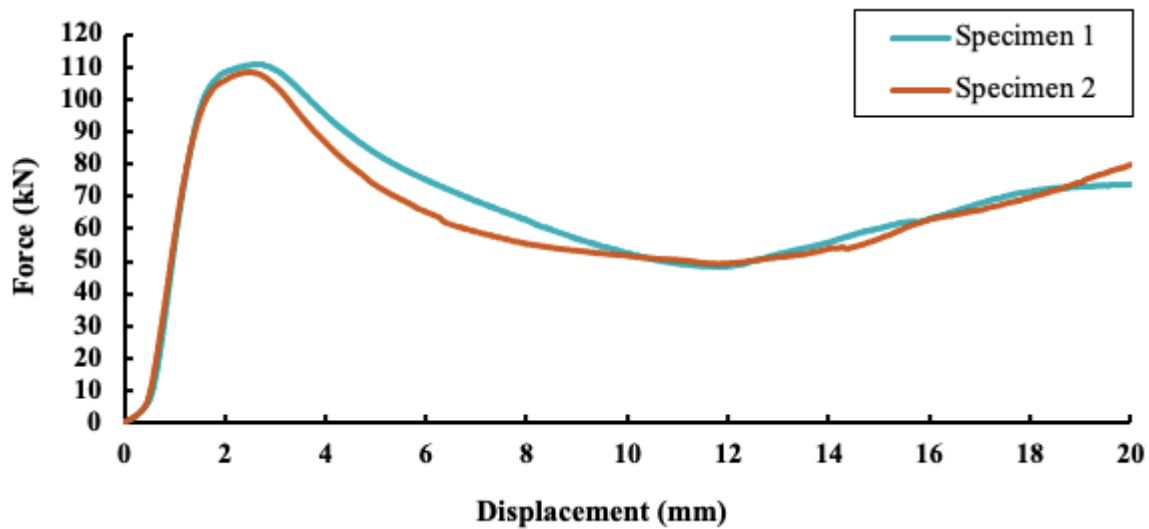


**Figure 4-14: C-F40 load-displacement plots**

Both curves have similar behaviors until the peak load. After that, both specimens behaved differently until 10 mm displacements, where the first specimen maintained a higher load. Then, the forces applied to the tubes were nearly equal until the tests were completed. Because this specimen configuration involved the crushing of tubes of such small lengths, these became very rigid at a small crushing displacement, and because of that, it is possible to notice a constant increase of force when they are crushed by about 30%. Although this can be characterized as the start of the densification region, it can be used for the crashworthiness analysis in order to maintain consistency between specimen configurations. Table 4-7 presents the calculated crashworthiness quantities.

**Table 4-7: C-F40 calculated quantities and discrepancy**

| Specimen | Mass (g) | $P_{max}$ (kN) | $P_{avg}$ (kN) | $E_c$ (kJ) | EA (kJ) | SEA (J/g) | CFE |
|---|---|---|---|---|---|---|---|
| 1 | 59.5 | 110.7 | 66.7 | 1.21 | 1.34 | 22.5 | 60.3% |
| 2 | 59.3 | 108.2 | 63.8 | 1.11 | 1.28 | 21.6 | 59.0% |
| Discrepancy | 0.3% | 2.3% | 4.4% | 7.9% | 4.5% | 4.2% | 1.3% |

These results indicate consistency between specimens. A difference of about 3 kN on the average crushing load was noticed and caused by the previously described slight force difference at a section of the load-displacement plots. Table 4-7 also presents the discrepancy between each of the calculated quantities. As seen, the greatest discrepancy is the energy absorbed under the post-crushing region, which is 7.9% between specimens.

Figure 4-15 shows that the foam helped avoid catastrophic failure due to wall deformation and to maintain consistency between specimens, similar to the other C-F configurations. The load-displacement plots and the crushing behavior show that progressive failure occurred. Also, the tubes were crushed up to a displacement of 20 mm, and the remaining 20 mm in length, is very rigid due to the compressed foam and aluminum.

**Figure 4-15: C-F40 crushing behavior**

## 4.3 SUMMARY OF EXPERIMENTAL RESULTS

The summary of the experimental results is presented in this section, which was divided into four parts based on the data. First, the effects of epoxy adhesion between the foam core and the tube wall on crashworthiness of aluminum tubes were compared. Second, the influence of the different reinforcements on the energy absorption capability of the tested tube configurations were analyzed. Third, the effects of changes in the L/D ratios of reinforced tubes on crashworthiness were assessed. Finally, design considerations were discussed.

### 4.3.1 Effects of the Adhesion of Foam Filled Cores on Crashworthiness

The effects of adhesives on crashworthiness of tubes were investigated through the testing of PVC foam-filled specimens with and without epoxy adhesion between the specimen's inner wall and the foam core. These are the A-FE120 and A-F120 specimen configurations, respectively. To maintain consistency between specimen configurations and allow for comparison, the same tube geometry was used throughout the tests (120 mm in length, 1.6 mm wall thickness, 60 mm inner diameter) and a 60 mm crushing displacement limit, or 50% of the specimen length. Figure 4-16 shows the load-displacement and absorbed energy plots for each configuration. It is important to note that the absorbed energy (EA) is the cumulative area under the force-displacement curve.
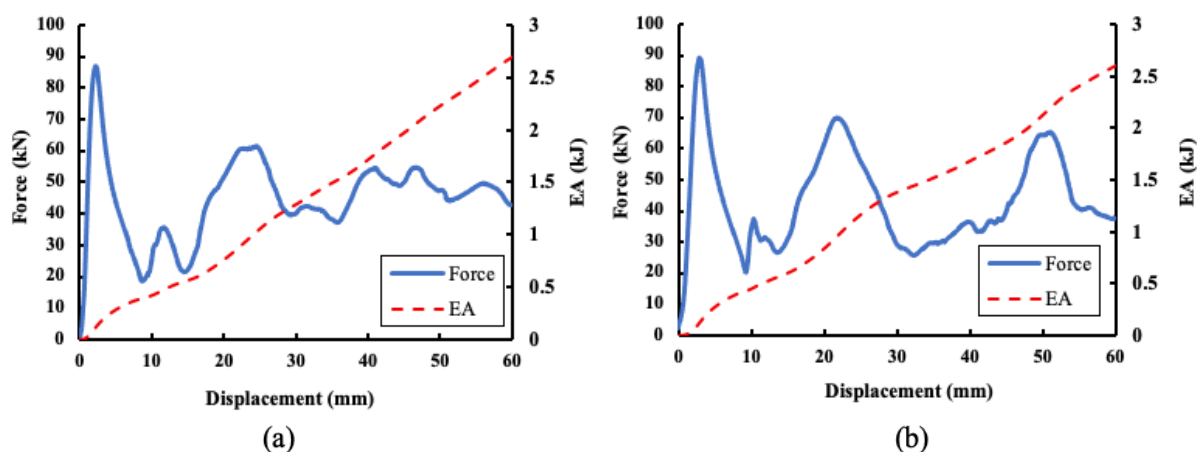
Figure 4-16: Load-displacement histories and absorbed energy for (a) A-F120, (b) A-FE120

As seen, the force-displacement curves had similar shapes, with high and low peak force values, which correspond to the movement of the tube wall during crushing. From Figure 4-16, it can be seen that the A-F120 specimen showed a lower peak load and a higher number of peaks throughout the post-crushing zone, especially after a displacement of 30 mm was achieved. On the other hand, the epoxied specimen showed higher values for upper and lower peaks during the post-crushing zone. Table 4-8 presents the mean crashworthiness quantities between the specimens for each configuration.

Table 4-8: Calculated crashworthiness quantities for A-F120 and A-FE120

| Configuration | Mass (g) | $P_{max}$ (kN) | $P_{avg}$ (kN) | $E_c$ (kJ) | EA (kJ) | SEA (J/g) | CFE |
|---|---|---|---|---|---|---|---|
| A-F120 | 132.1 | 87.1 | 43.0 | 2.48 | 2.58 | 19.5 | 49.4% |
| A-FE120 | 144.0 | 88.8 | 42.1 | 2.40 | 2.58 | 17.9 | 47.6% |

By comparing these quantities, it is possible to confirm that the epoxy adhesion increased the peak load by almost 2 kN due to the epoxy bond, which was maintained at the external foam layer, causing the foam to crack at that location, as seen in Figure 4-17. Since the foam failed before the epoxy at that location, it could be concluded that the adhesive used was stronger than the foam, as recommended by the manufacturer [38].

From the derived quantities, it is also noticed the non-epoxied configuration demonstrated a higher crush force efficiency due to its higher average crushing load and a higher energy absorption on the post-crushing zone. The difference of almost 12 grams between configurations due to the adhesive, resulted in a smaller specific energy absorption for the epoxied tube. Also, because both the specific energy absorption and the average crushing load were smaller for the epoxied configuration, as the specimen suffers further displacement, its specific energy absorption is expected to further decrease. The decrease in this value was not justified by a considerable energy absorption increase. In fact, the adhesive did not improve the total absorbed energy as this quantity remained at 2.58 kJ for both configurations. Figure 4-17 shows the crushed A-F120 and A-FE120 specimens.



(a)  (b)
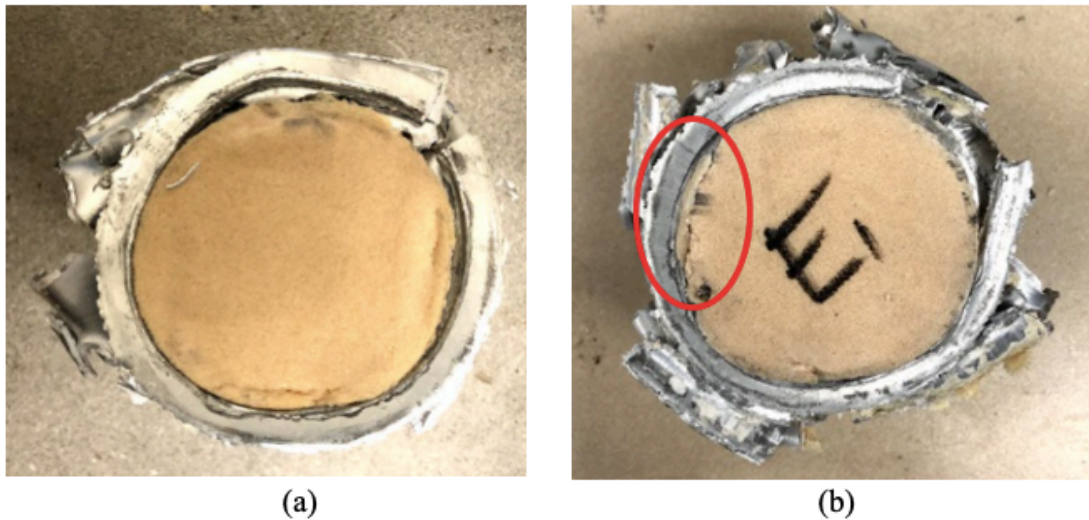
**Figure 4-17: Crushed specimens (a) A-F120, (b) A-FE120**

As previously mentioned, the foam resisted inwards wall buckling on both configurations, as expected. While the bond between the foam and the tube wall was maintained and outward wall movement was prevented at some locations, which explains the smaller number of peaks throughout the post-crushing zone in the load-displacement plot [21], the epoxy failed at some locations. Because the foam was manually cut, trimmed, and inserted inside the tube, a partially rough surface was created on the perimeter of the foam layers, along their thickness. Due to this uneven periphery, the epoxy did not bond the foam with the tube wall properly, and failed. At the locations where smoother surface was achieved, wall movement was

resisted by this bond. Figure 4-18 shows the difference in roughness between the surfaces in a foam layer. For proper foam adhesion, nearly impeccable surfaces, such as the one shown are necessary. The shown smooth surface was prepared by the manufacturer and is the one commonly bonded to outer cores of sandwich panels [38]. Through the analyses of the presented crashworthiness quantities and crushing behavior, it is concluded that using adhesives to provide a bond between the foam core and the tube did not make enough difference on the crashworthiness of aluminum tubes. For this study the specimens are manually prepared and perfectly smooth surfaces along the periphery of foam layers are infeasible, therefore non-epoxied foam-filled cores were selected for the other investigations.
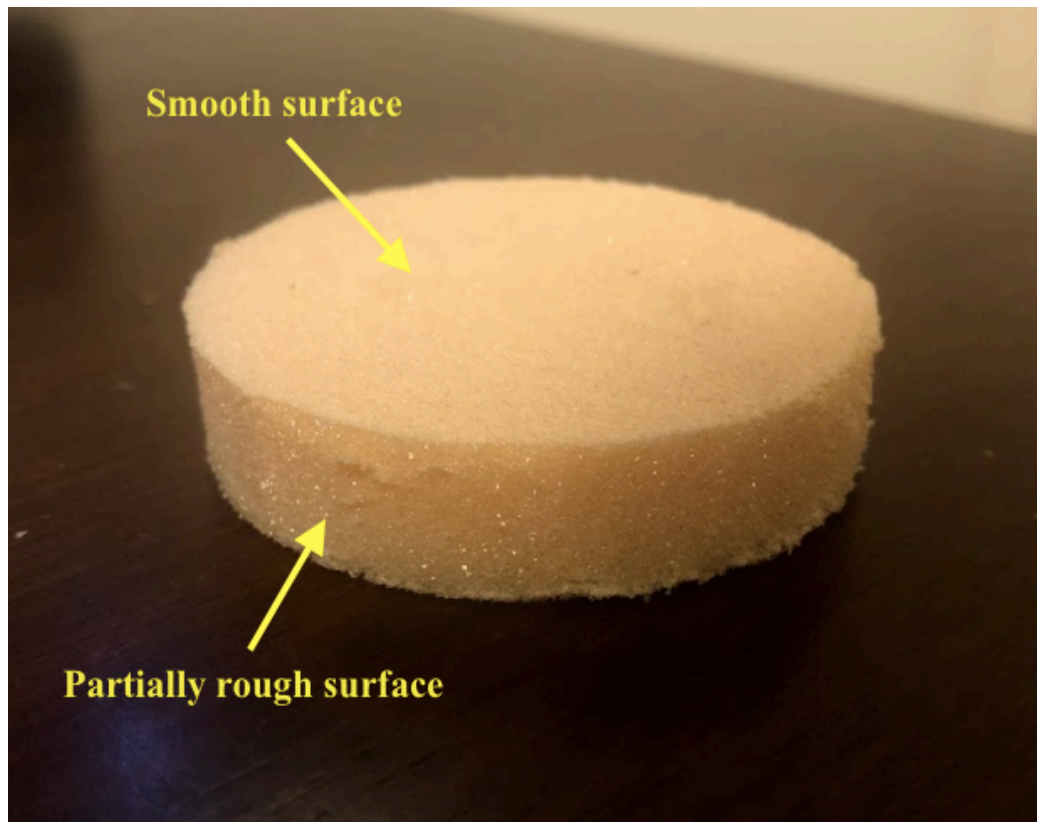


**Figure 4-18: PVC foam surfaces**

**4.3.2 Influence of CFRP and Foam Core Reinforcements on Crashworthiness**

To investigate the effects of CFRP and PVC foam core reinforcements on the crashworthiness of aluminum tubes, tubes of different reinforcement configurations were tested under quasi-static axial loads. These are:

- Hollow aluminum tube (A-H120) – "control" configuration.
- Hollow aluminum tube with CFRP reinforcement (C-H120).
- PVC foam-filled aluminum tube (A-F120).
- PVC foam-filled aluminum tube with CFRP reinforcement (C-F120).

To maintain consistency between specimen configurations, the same tube geometry was used throughout the tests (120 mm in length, 1.6 mm wall thickness, 60 mm inner diameter) and a crushing displacement limit of 50% the initial tube height, or 60 mm. It is important to note that the CFRP reinforced tubes have an additional 1.6 mm wall thickness due to the four layers of 0.4 mm each. The load-displacement and energy absorbed plots for each configuration are shown in Figure 4-19.
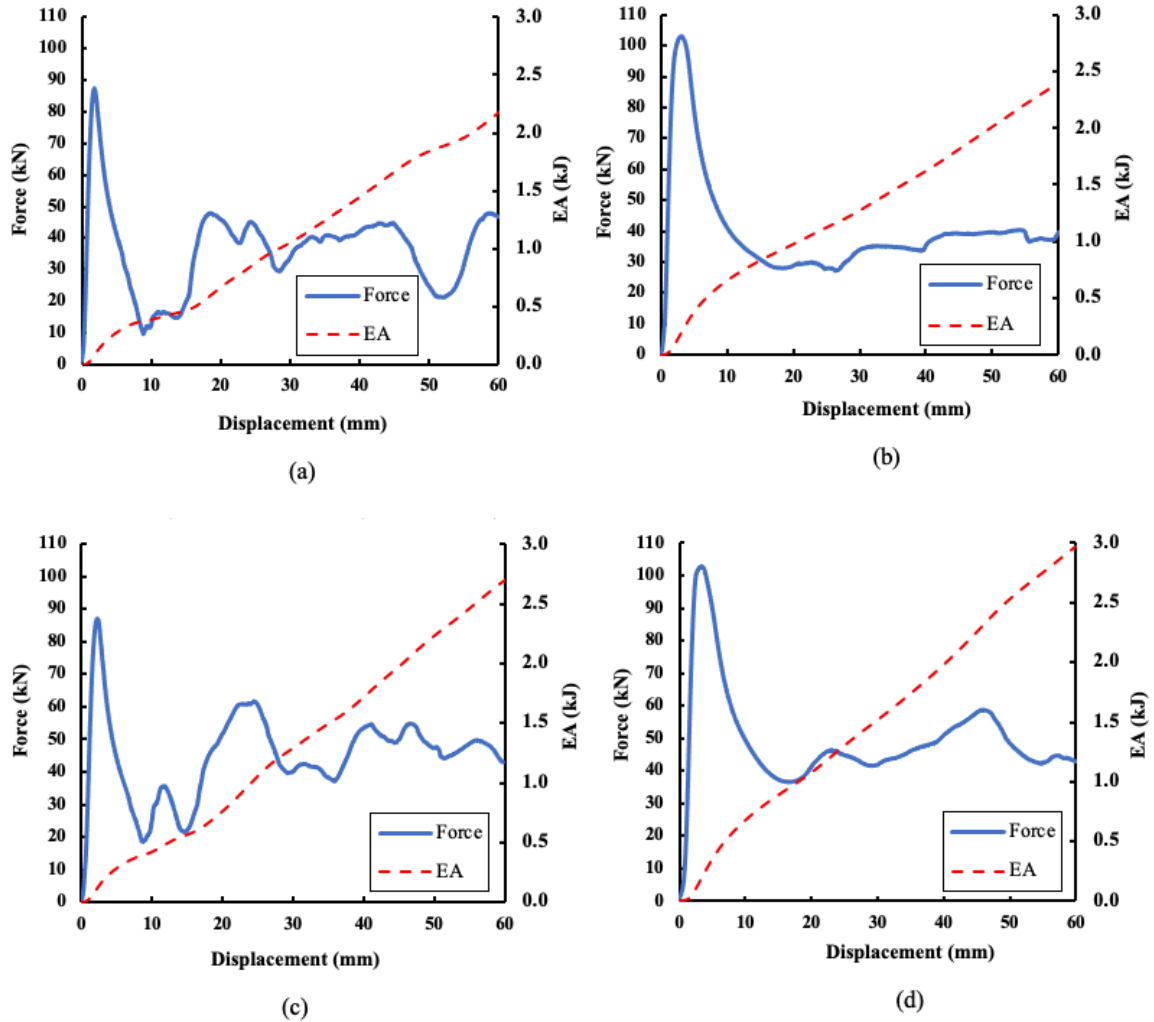
**Figure 4-19: Load-displacement and absorbed energy plots for (a) A-H120, (b) C-H120, (c) A-F120, (d) C-F120**

As investigated by to Yalçın et al. [21], it is possible to notice that CFRP reinforcement does, indeed, change the oscillation of the load-displacement curves during the post-crushing zone. A more plateau-like behavior of these curves was observed for the specimen configurations that include this reinforcement. According to Eksi et al. [26]. This behavior is preferred as a nearly constant plateau means a higher load efficiency is achieved. Also, this reinforcement improves the maximum peak load and reduces the slope of the loading softening after this peak load is achieved. In that region, for the C-H120 and C-F120, more stable curve behavior was observed due to the rigidity and strength the CFRP adds to the wall of the tubes. The PVC foam, on the other hand, did not alter the oscillation of the curve. During the post-crushing zone each of the high and low peaks were shifted up by the foam by up to 20 kN and the curve was shifted up by 7 kN in average. This causes a considerable increase in energy absorption

for the specimen and is mainly due to the wall support that the foam provides, restraining the wall from inward movement. This increase in force during the post-crushing was also observed by Yalçın et al. [21]. The comparison between these curves is seen in Figure 4-20. The PVC foam, by itself did not affect the maximum peak load and did not alter the first negative slope seen in the plot.
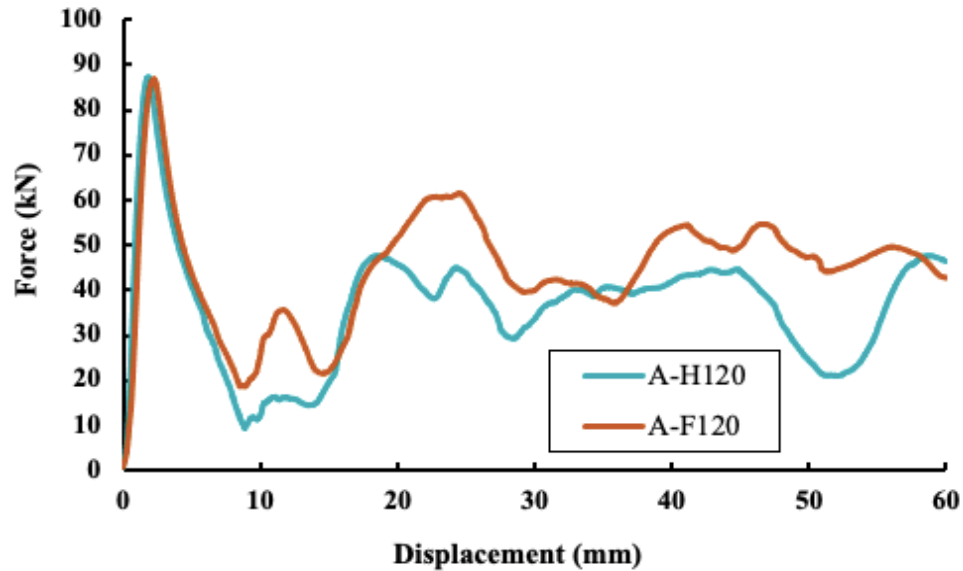


Figure 4-20: A-H120 vs. A-F120 load-displacement curves

The crashworthiness quantities for each of the four configurations are shown in Table 4-9. The C-H120 configuration was found to be unpredictable with such specimen height as wall buckling occurred. However, one of its specimens had results that are worth noticing which are included in the table. The remaining values in the table were mean quantities between the tested specimens.

Table 4-9: Crashworthiness quantities for tubes of 120 mm in length

| Configuration | Mass (g) | $P_{max}$ (kN) | $P_{avg}$ (kN) | $E_c$ (kJ) | EA (kJ) | SEA (J/g) | CFE |
|---|---|---|---|---|---|---|---|
| A-H120 (control) | 106.2 | 87.3 | 35.9 | 2.09 | 2.18 | 20.5 | 41.1% |
| C-H120 | 154.3 | 103.3 | 38.6 | 2.19 | 2.39 | 15.5 | 37.3% |
| A-F120 | 132.1 | 87.1 | 43.0 | 2.48 | 2.58 | 19.5 | 49.4% |
| C-F120 | 178.8 | 104.7 | 48.9 | 2.78 | 2.97 | 16.6 | 46.7% |

As seen, the CFRP reinforcement increases the mass of the specimen by roughly 48 grams, or 45%, while the foam increases it by about 26 grams, or 24%. The CFRP reinforcement increased the peak force of the specimen. In fact, this reinforcement alone aided in an increase of about 16 kN, or 18% in this quantity. Because the foam did not aid in an increase in peak force, by combining both reinforcements, the peak load was substantially increased compared to the CFRP reinforced tube, alone. An increase of 1.5 kN for this value was observed by adding the foam to the CFRP reinforcement. Because of that, it is concluded that both specimens together improved this quantity than either of the reinforcements alone.

As previously noted, in spite of the catastrophic failure observed for the C-H120 configuration, it is still worth comparing its results with the other configurations. The peak force, for example, was not affected by the deformation mode as failure occurs after that point in the load-displacement plot. In addition, in spite of wall buckling, the CFRP reinforcement aided in an increase in average crushing force of about 3 kN, or 7%, in comparison with the control configuration. A more substantial improvement in this quantity was noticed by the application of PVC foam as the average crushing force was increased by 7 kN, or 19.5%, in comparison with the hollow aluminum tube. For the C-F120 configuration, by combining both reinforcements, this value is increased by 13 kN, or 36%, which is a considerable increase.

Another result that is worth discussing is the total energy absorbed for each specimen configuration throughout the crushing. This is the cumulative area under the load-displacement plot. Even with the undesired wall buckling caused by the CFRP on the unfilled core configuration, this reinforcement increased this value by 213 J, or by almost 10% comparing to the control tube. The foam reinforcement caused a more substantial increase in energy absorption. By shifting up the load-displacement curve on the post-crushing zone, this value was improved by 403 J, or 18.5%, in relation to the control tube. By combining both reinforcements, for the C-F120 configuration, an improvement of almost 800 J was observed. This corresponds to a 36.6% improvement. Therefore, an additional 180 J energy was absorbed through the combination of both reinforcements. Although the performance of the C-H120 was affected by wall buckling, it is important to point out that this additional energy is absorbed due to the complementary influence these reinforcements have in the aluminum tube. This is because, the CFRP restrains the wall movement outwards, while the foam

restrains it inwards. In addition, the CFRP provided a more plateau-like load-displacement in the post-crushing zone, as previously mentioned. This also helped in an improvement in load efficiency. A comparison between the cumulative energy absorbed throughout the test for each configuration is seen in Figure 4-21. It is important to note that the total energy absorbed is the point where the lines intersect the y-axis, at 60 mm displacement.
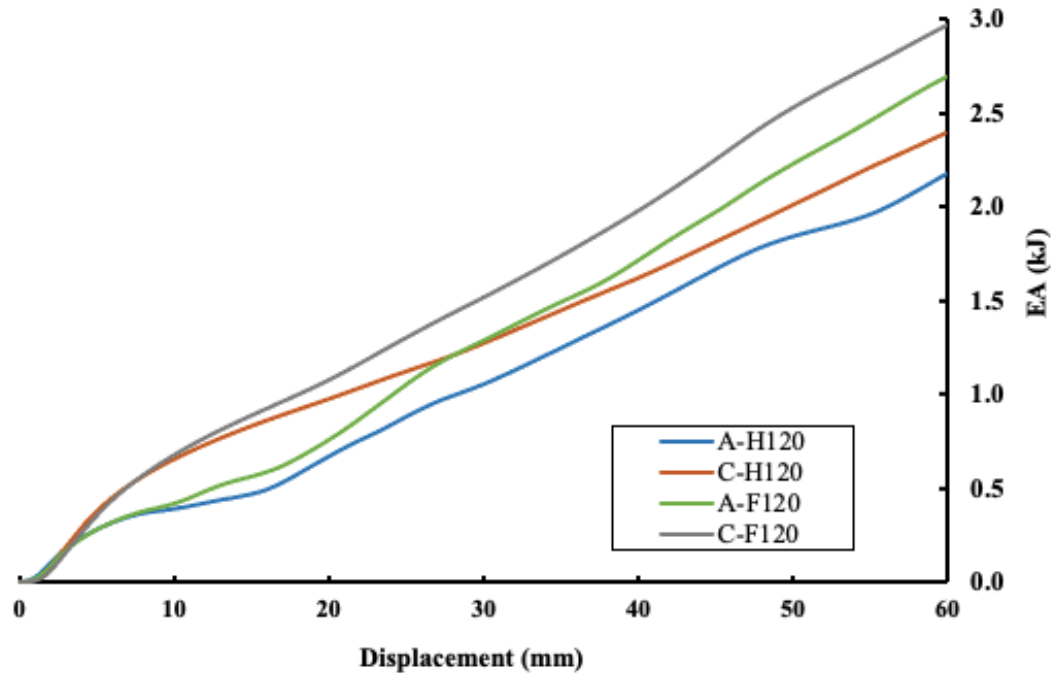


**Figure 4-21: Absorbed energy for specimens of 120 mm in length**

Although it is noticeable an improvement in most quantities with the addition of the investigated reinforcements, the specific energy absorption was found to decrease with more provided reinforcements. This contradicts the findings from Yalçın et al. [21], in which was observed that the specific energy absorption of specimens increased with the addition of PVC foam and CFRP reinforcements. However, for that study specimens of 50 mm in length were investigated and the aluminum used was about 48% lighter per unit length. This difference in tube mass per unit length was due to an aluminum properties and tube geometries. Because of this, the tube in that research was much weaker without reinforcement. For example, according to Yalçın et al., the addition of CFRP increased the peak load by approximately

75%, achieving around 70 kN with this reinforcement, which is much smaller than what was found in this study. Since the aluminum tube used for this research was much stronger by itself, the addition of reinforcements did not increase specific energy absorption. In other words, the increase in mass by the addition of reinforcements is greater than the increase in energy absorption achieved with these reinforcements. In addition, for this study, the total energy absorption values found were for 50% crushing displacements. Tall specimens such as the ones used for this investigation were capable of suffering further crushing before they achieve the densification region. Because of this, the specific energy absorption becomes greater as specimens are further displaced. Also, with a high average crushing force, as found in this study, the specific energy absorption is expected to increase at a consistent, considerably high rate as the specimens are further displaced.

Figure 4-22 shows the load-displacement curves for the control hollow aluminum tube and for the PVC foam core and CFRP reinforced aluminum tubes. As shown, in the maximum peak force region, the peak force was increased mainly due to the CFRP reinforcement and the decrease in loading after this force was much steadier, presenting a smaller slope throughout the transition to the plateau region of the plot. In the post-crushing zone, the CFRP reduced the oscillation of the curve, creating a more consistent plateau-like behavior. The PVC foam shifts up the load-displacement curve during the post-crushing zone. This generates a greater energy absorption throughout that region. Also, PVC foam reinforcement assists with the predictability due to the core support it provides.
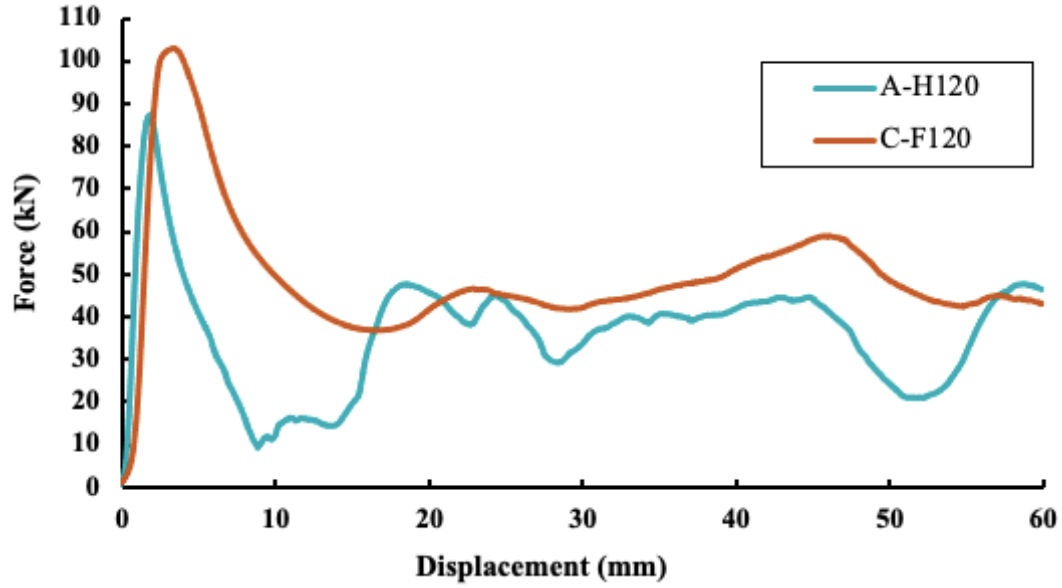
**Figure 4-22: A-H120 vs. C-F120 load-displacement curves**

### 4.3.3 Effects of the L/D Ratio Alteration of Reinforced Tubes on Crashworthiness

The following specimen configurations were tested under quasi-static axial loads:

- C-F40: 40 mm in length and L/D = 0.67
- C-F80: 80 mm in length and L/D = 1.33
- C-F120: 120 mm in length and L/D = 2.00

This was done to investigate the effectiveness of the combined PVC foam and CFRP reinforcing configuration in aluminum tubes of different length-to-diameter ratios (L/D). All of these tubes have a constant inner diameter of 60 mm and wall thickness of 1.6 mm. It is important to note that the CFRP reinforcement adds an additional 1.6 mm in wall thickness. For consistency, all configurations were tested until a crushing displacement equal to 50% of the initial specimen length was achieved. Figure 4-23 shows the load-displacement plots for each of these configurations.
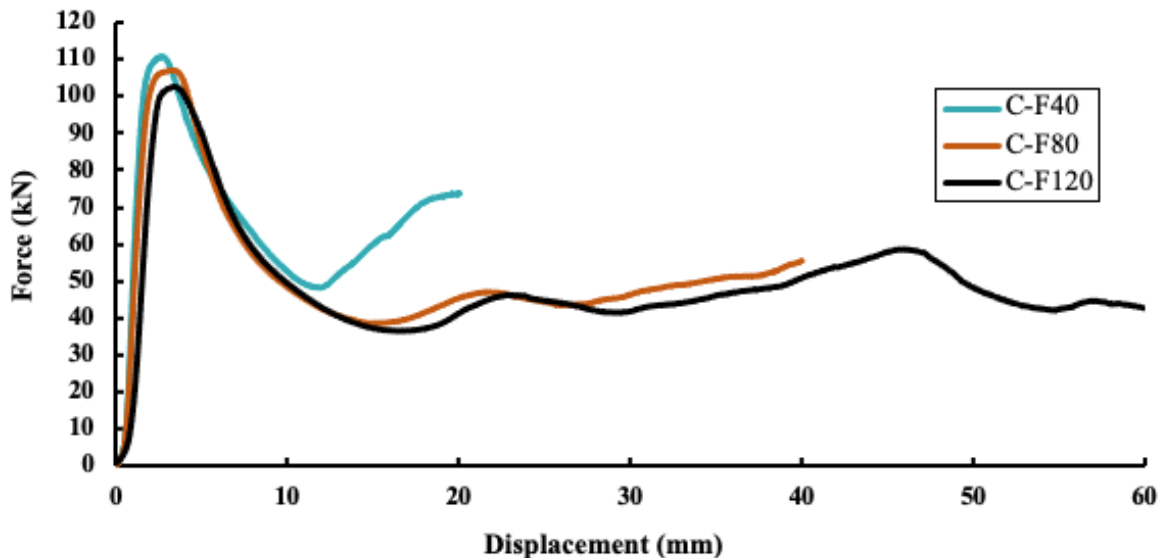
**Figure 4-23: Load-displacement plots for reinforced tubes of different L/D ratios**

As seen, the behavior of the curves in the peak force zone was similar. The smaller the L/D ratio, the greater was the slope in the linear-elastic, pre-crushing, region of the plot. The 40-mm long tube reached its densification zone immediately after the force dropped from its peak force, while the tubes of 80 mm and 120 mm behave similarly throughout the post-crushing zone up to 50% crushing. These two configurations had plateaus at a very similar force. For comparison, Figure 4-24 presents the load versus percent crushing for the tested tubes of different L/D ratios.
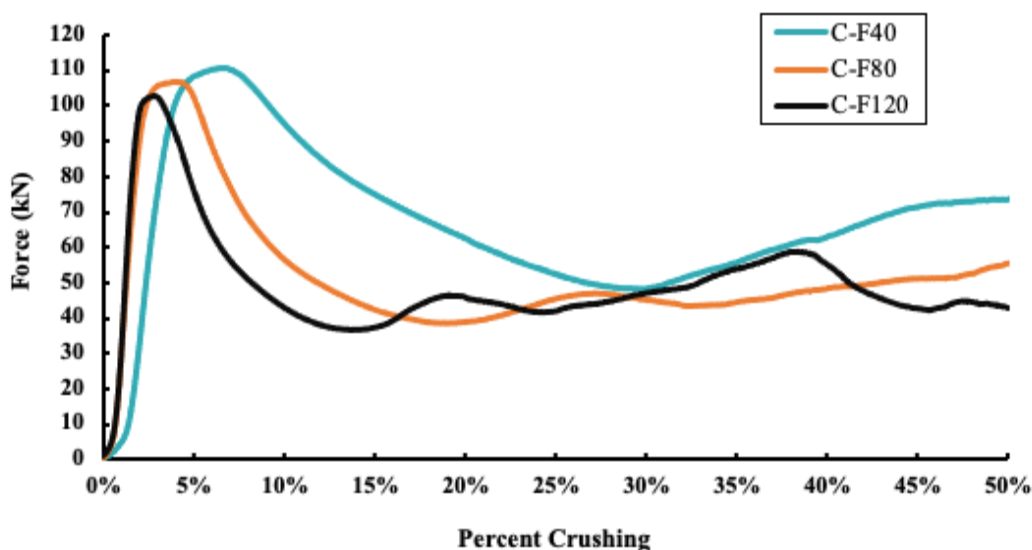


**Figure 4-24: Load vs. percent crushing plots for reinforced tubes of different L/D ratios**

From the load-displacement plots, crashworthiness quantities for each of the specimen configurations could be calculated and are shown in Table 4-10.

Table 4-10: Crashworthiness quantities for reinforced tubes of different L/D ratios

| Configuration | Mass (g) | $P_{max}$ (kN) | $P_{avg}$ (kN) | $E_c$ (kJ) | EA (kJ) | SEA (J/g) | CFE |
|---|---|---|---|---|---|---|---|
| C-F40 | 59.4 | 109.4 | 65.3 | 1.16 | 1.31 | 22.0 | 59.6% |
| C-F80 | 119.1 | 106.2 | 49.3 | 1.82 | 2.04 | 17.1 | 46.4% |
| C-F120 | 178.8 | 104.7 | 48.9 | 2.78 | 2.97 | 16.6 | 46.7% |

First, as expected, the mass per unit length for all specimens were nearly the same; the specimen of 80 mm in height had roughly twice the mass of the one of 40 mm. Also, the 120-mm long specimen had around three times the mass of the smallest specimen. This confirms the consistency in the specimen preparation as all three configurations were assembled with the same reinforcements and consisted of the same material properties. Comparing the calculated quantities, it was observed that the peak force increased as the L/D ratio decreased. Increasing the tube length from 40 mm to 80 mm, reduced the peak force by about 3 kN. Increasing the tube length from 80 mm to 120 mm, reduced the peak force by 1.5 kN. This increase in peak force for smaller specimens was expected as the rigidity of a specimen decreases as its length increases.

For the remaining quantities the specimens of 120 mm and 80 mm have very similar values. The smaller specimen reached densification and its rigidity caused the applied force to increase substantially still at roughly 30% crushing. Because of that, the smaller specimen showed theoretically superior results during the 50% crushing window.
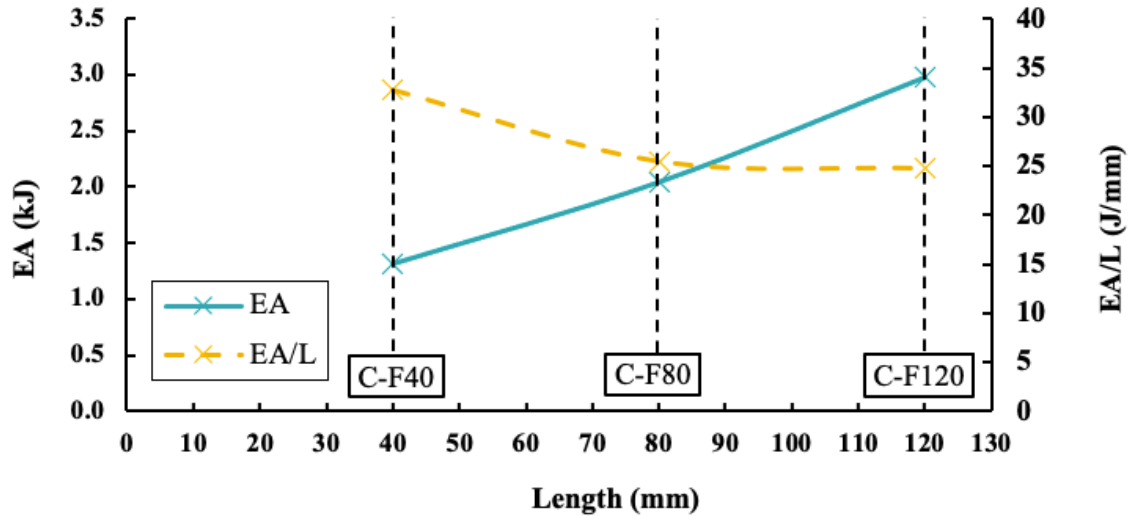
**Figure 4-25: EA and EA/L for reinforced tubes of different lengths**

As seen in Figure 4-25, the total absorbed energy increases almost linearly with the increase in length. This demonstrates that the combined PVC foam and CFRP reinforcing configurations have equal energy absorption efficiency for tubes with lengths between 40 mm and 120 mm. Also, as presented, these tubes presented predictable and similar failure modes during testing, which confirms uniformity between tubes of different lengths. On the other hand, it is possible to note that tubes of 40 mm in length has higher energy absorbed per unit length than the other two configurations. This is because of its densification region that starts within the 50% crushing window. It is important to note that the peak force slightly decreases with the increase in tube length, although the available energy is increased. This decrease in peak force, however, can be considered negligible as there is a substantial increase in energy absorption. In addition, it is important to note that taller tubes can substantially increase the weight of the system and become unfeasible for the design of some retrofitting structures.

Yalçın et al. [21] investigated the crashworthiness of PVC foam and CFRP reinforced aluminum tubes of 50 mm in length, wall thickness of 1.25 mm and diameter of 56 mm. In addition to different aluminum properties, that study investigated tubes of much smaller diameter-to-wall thickness ratio (D/t). The D/t ratio is another important geometric parameter that controls the crashworthiness performance and failure modes of aluminum tubes in combination with the L/D ratio [15]. Yalçın et al. investigated tubes of D/t = 44.8 while for

this research the investigation was conducted on constant D/t ratio of 37.5. This reduction of about 20% in the D/t ratio, in combination with a different aluminum used, show inferior crashworthiness resuts than the ones found in this study. For example, the specimens designed by Yalçın et al. absorbed 1645 J when crushed 37 mm. When the C-F80 specimen was crushed same 37 mm, the tube absorbed 1925 J. This is an improvement of about 17%. With regards to peak load, the specimens developed by Yalçın et al. supported a maximum peak force of about 80 kN, while the C-F80 specimen designed in this study supported a maximum peak force greater than 106 kN. This is a 33% improvement for a specimen that is 30 mm longer. As investigated, with the designed reinforced tube configuration, the peak load increases by 0.3% for every decrease in 10 mm in tube length for tubes between 40 mm and 80 mm. However, the specimens for this research are 48% heavier per unit length in comparison to the one designed by Yalçın et al.

**4.3.4 Design Considerations for PVC Foam and CFRP Reinforced Tubes**

When designing energy absorbing structures, it is necessary to consider factors such as constructability, weight, and cost, in addition to performance. With proper automation, the constructability of PVC foam and CFRP reinforcements can be significantly improved and as these materials become more popular, skilled labor is expected to become more inexpensive. In addition to great crashworthiness characteristics and performance, these reinforcing materials offer superior workability compared to other reinforcement methods such as the welding of stiffeners or honeycomb. As seen in Table 4-11, PVC foam and CFRP are relatively expensive materials in comparison with aluminum. This is because the use of these materials is relatively recent, especially in structural application. For example, carbon fibers, are expected to decrease cost in the upcoming years, due to the development of low-cost and high-yield precursors for manufacture of these materials [45].

**Table 4-11: Material cost for aluminum, carbon fiber, epoxy, and PVC foam**

| Material Quantity | Aluminum [46] | Epoxy [47] | Carbon Fiber [45] | PVC Foam [48] |
|---|---|---|---|---|
| Per kg | $4.50 | $24.99 | $21.50 | $35.77 |

The approximate material cost, based on the current market value, for of each of the investigated specimen configurations is shown in Table 4-12. It is important to note that the price is proportional to the length of the specimens. Therefore, C-F80 and C-F40 would cost $1.66 and $0.83, respectively.

Table 4-12: Material cost per configuration

| - | A-H120 | C-H120 | A-F120 | C-F120 |
|---|---|---|---|---|
| Cost per tube | $0.48 | $1.56 | $1.40 | $2.49 |

To put it into perspective, consider the face of the structure shown in Figure 4-26. Using two aluminum outer plates of 2 mm and an energy absorber core comprised of C-F120 tubes staggered as shown in Figure 4-27, the material cost for the sacrificial cladding would be of approximately $53,000. The panels would impose an additional 300 lb/ft dead load to the exterior girders in any floor level of the structure. This cladding structure would consist of approximately 22 psf dead load, which is much lighter than an exterior stud wall with brick veneer, for example, which has a design dead load of 48 psf [49].
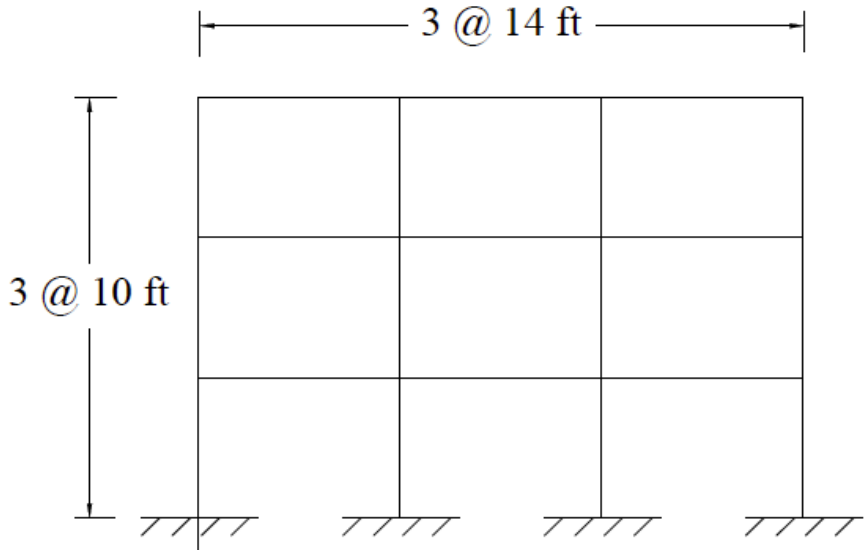


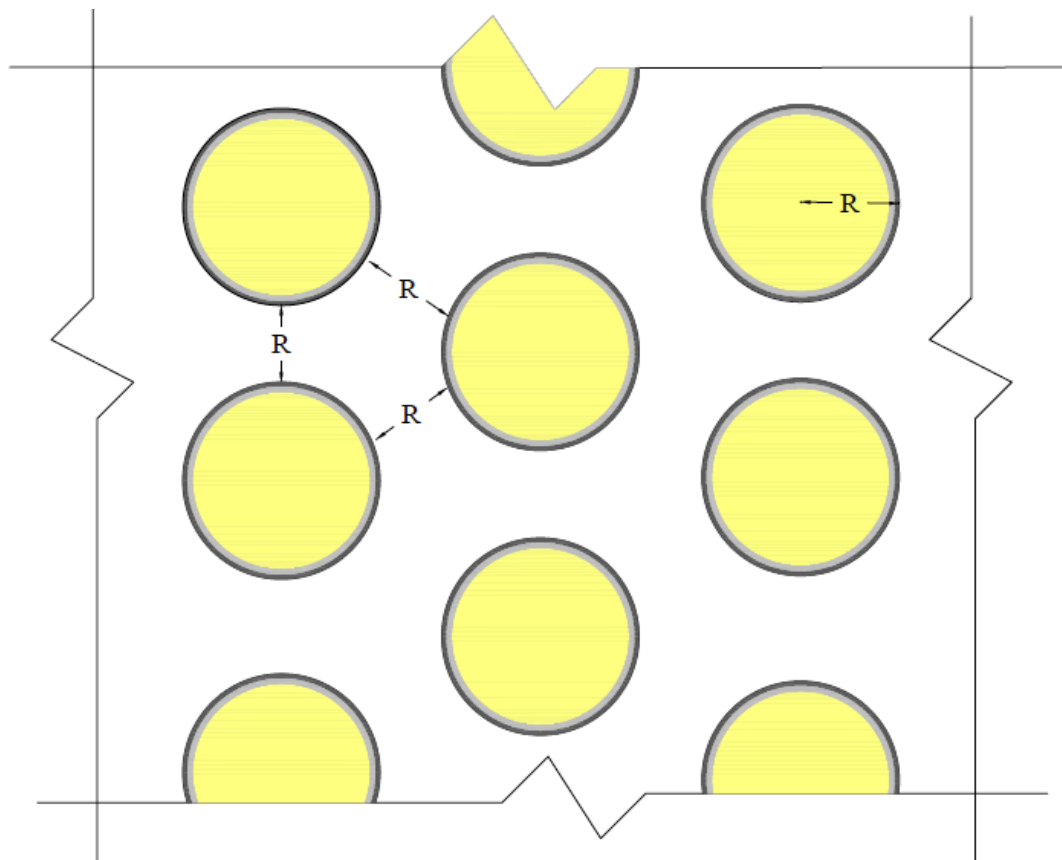Figure 4-26: Illustrative structure

**Figure 4-27: Illustrative sacrificial cladding core layout**

# CHAPTER 5: CONCLUSIONS AND RECOMMENDATIONS

The first objective of this study was to investigate the effects of the use of foam-filled core adhesives in the crashworthiness of thin-walled aluminum tubes through quasi-static axial tests of tubes with and without an epoxy bond between the tube wall and the foam core. It was found that the use of the adhesive does not improve the crashworthiness of the specimen. In fact, it adds 9% more mass to the specimen, while the post-crushing quantities remain nearly unaltered. This is because a achieving a perfectly smooth foam surface for proper epoxy adhesion is unfeasible during manual assembly of tubes with this core reinforcement. The only improvement observed due to the epoxy adhesion was the increase in peak force by 2%, while restraining outward wall movement at locations along the tube length where appropriate foam surface for adhesion was provided.

The next goal of this research was to investigate the effects of CFRP and PVC foam reinforcements in the crashworthiness of tall aluminum tubes of L/D = 2 and 120 mm in length. Through the testing of specimens with different specimen reinforcing configurations, it was found that CFRP with [0°/90°/0°/90°] orientation provides a substantial increase in peak load while changing the oscillation of the load-displacement curve to a more plateau-like behavior. On the other hand, if no core reinforcement is provided, the tube's wall tend to move inwards, causing wall buckling, which reduces the post-crushing zone crashworthiness quantities and increases the unpredictability of this configuration. The PVC foam restrains inward wall movements and shifts up the load-displacement curve in the post-crushing zone, increasing energy absorption. In addition, this reinforcement was found to be complementary to CFRP, since the combination of CFRP wrapping and PVC foam cores provides both inward and outward wall supports, increasing the crashworthiness performance of the aluminum tubes.

Next, the effects of L/D ratio on the crashworthiness of CFRP and PVC foam reinforced tubes were investigated. By testing tubes of 60 mm inner diameter and varying lengths (40 mm, 80 mm, and 120 mm), it was found that the potential energy absorption was proportional to tube length and the peak load was inversely proportional to tube length due to an increase in rigidity. It was shown that the CFRP and PVC foam reinforced configuration is effective for tubes of varying lengths, especially for tubes with lengths between 80 mm and 120 mm. This

is because it was found that the specimen of 40 mm in length and L/D = 0.67 achieved densification at a 30% crushing, demonstrating a short post-crushing region. Although it is expected that this combination of reinforcements provides outstanding wall support and predictability for tall aluminum tubes, tubes longer than 120 mm will cause a considerable increase in weight to the retrofitted structure. The design of a retrofitting structure is a tradeoff between potential energy absorption, cost, and structural feasibility. With proper structural analysis of the building prior to the sacrificial cladding installation, it is possible to determine how much additional load a structure is able to accommodate and select the ideal core design.

After completing the experimental testing of aluminum tubes for energy absorbing applications, the summary of findings is as follows:

- Epoxy adhesion between the PVC foam core and the tube wall increased the peak load by 2%.
- Epoxy adhesion between the PVC foam core and the tube wall had no effects on absorbed energy.
- CFRP reinforcement increased the peak load of aluminum tubes by 18% and changed the oscillation of the load-displacement plot in the post-crushing zone to a more plateau-like behavior.
- PVC foam shifted up the load-displacement curve by 7 kN on average, increasing the energy absorption of tubes by 18.5%.
- Aluminum tubes with CFRP and PVC foam reinforcements had almost 37% higher total energy absorption than the control tube and 20% higher peak load. This was found to be the best configuration with respect to energy absorption capability and crashworthiness behavior due to use of complementary reinforcing materials.
- The peak load was increased by 4.5% for CFRP and PVC foam reinforced tubes of 40 mm in length in comparison with ones of 120 mm. Peak load for tubes of 80 mm in length was about 2% greater than the ones of 120 mm.
- The absorbed energy throughout 50% crushing of CFRP and PVC foam reinforced tubes is proportional to the increase in specimen length.

- CFRP and PVC foam reinforced tubes of 40 mm in length (L/D = 0.67) were found to achieve densification at about 30% crushing, which demonstrates a short post-crushing region.

The following list is a set of recommendations for future studies:

- Investigate the crashworthiness performance of CFRP and PVC reinforced tubes as a system to simulate a section of a sacrificial structure, and select the most efficient arrangement.
- Investigate the effects of moisture in the performance of aluminum tubes with PVC foam-filled cores.
- Investigate the contribution of CFRP and PVC reinforcement in tubes of varying wall thicknesses and diameters.
- Investigate the contribution of these reinforcements in tubes of different shapes such as square and other polygonal shapes.
- Investigate the use of foam in multi-cell tube cores.
- Investigate the effects of using different number layers of CFRP and orientations in combination with PVC foam.
- Investigate the performance of PVC foam reinforcement in combination with different FRPs, simultaneously.
- Investigate the effects of foam density in FRP reinforced tubes.
- Investigate and select the most efficient radially graded foam core configuration to be used with FRP reinforced tubes.

# REFERENCES

[1] Codina, R., D. Ambrosini, F. de Borbon. "New sacrificial cladding system for the reduction of blast damage in reinforced concrete structures." *International Journal of Protective Structures*, 8(2):221-236, 2017.

[2] FBI. "Oklahoma City bombing." https://www.fbi.gov/history/famous-cases/oklahoma-city-bombing.

[3] The New York Times. "Drone strike kills planner of 2008 Islamabad Hotel bombing, U.S. says." 2017. https://www.nytimes.com/2017/03/26/us/qari-yasin-killed-2008-islamabad-hotel-bombing.html.

[4] CNN. "Investigators are looking at 'any and all possible motives' after identifying Nashville bomber." 2020. https://www.cnn.com/2020/12/28/us/nashville-bomb-christmas-monday/index.html.

[5] Nature. "Why Beirut's ammonium nitrate blast was so devastating." 2020. https://www.nature.com/articles/d41586-020-02361-x.

[6] Vinson, J. R. "Sandwich structures." *Appl. Mech. Rev.*, 54(3): 201-214, 2001.

[7] Thinvongpituk, C., N. Onsaloong, S. Poonaya. "Crush characteristic of foam-filled circular steel and aluminum tubes under axial loading." *Conference: Proceedings of the World Congress on Engineering*, vol. 2, 2016.

[8] Mamalis, A. G., D. E. Manolakos, M. B. Ioannidis, D. P. Papapostolou. "Crashworthy characteristics of axially statically compressed thin-walled square CFRP composite tubes: experimental." *Composite Structures*, 63(3-4):347–360, 2004.

[9] Van Paepegem, W., S. Palanivelu, J. Degrieck, J. Vantomme, B. Reymen, D. Kakogiannis, J. Wastiels, D. Van Hemelrijck. "Blast performance of a sacrificial cladding with composite tubes for protection of civil engineering structures." *Composites Part B: Engineering*, 65:131-146, 2014.

[10] Alexander, J. M. "An approximate analysis of the collapse of thin cylindrical shells under axial loading." *The Quarterly Journal of Mechanics and Applied Mathematics*, 13(1):10–15, 1960.

[11] Lau, S. T. W., M. R. Said, M. Y. Yaakob. "On the effect of geometrical designs and failure modes in composite axial crushing: A literature review." *Composite Structures*, 94(3):803–812, 2012.

[12] Ma, J., Y. Yan. "Quasi-static and dynamic experiment investigations on the crashworthiness response of composite tubes." *Polymer Composites*, 34(7):1099–1109, 2013.

[13] Yan, L., N. Chouw. "Crashworthiness characteristics of flax fibre reinforced epoxy tubes for energy absorption application." *Materials and Design*, 51:629–640, 2013.

[14] Tarlochan, F., S. Ramesh. "Composite sandwich structures with nested inserts for energy absorption application." *Composite Structures*, 94(3):904–916, 2012.

[15] Guillow, S. R., G. Lu, R. H Grzebieta. "Quasi-static axial compression of thin-walled circular aluminum tubes." *International Journal of Mechanical Sciences*, 43(9): 2103-2123, 2001.

[16] Abada, M., A. Ibrahim. "Hybrid multi-cell thin-walled tubes for energy absorption applications: Blast shielding and crashworthiness." *Composites Part B: Engineering*, vol. 183, 2020.

[17] Alavi Nia, A., M. Parsapour. "Comparative analysis of energy absorption capacity of simple and multi-cell thin-walled tubes with triangular, square, hexagonal and octagonal sections." *Thin-Walled Structures*, 74:155-165, 2014.

[18] Zhang, H., X. Zhang. "Crashworthiness performance of conical tubes with nonlinear thickness distribution." *Thin-Walled Structures*, 99:35-44, 2016.

[19] Wu, S., G. Li, G. Sun, X. Wu, Q. Li. "Crashworthiness analysis and optimization of sinusoidal corrugation tube." *Thin-Walled Structures*, 105:121-134, 2016.

[20]  Nagel, G. M., D. P. Thambiratnam. "A numerical study on the impact response and energy absorption of tapered thin-walled tubes." *International Journal of Mechanical Sciences*, 46(2):201-216, 2004.

[21]  Yalçın, M. M., K. Genel. "On the axial crush performance of PVC foam-filled aluminum/CFRP hybrid circular tube." *Sakarya University Journal of Science*, 23(6):1154–1162, 2019.

[22]  Santosa, S., T. Wierzbicki. "Crash behavior of box columns filled with aluminum honeycomb or foam." *Computers & Structures*, 68(4):343–367, 1998.

[23]  Santosa, S., T. Wierzbicki. "Effect of an ultralight metal filler on the bending collapse behavior of thin-walled prismatic columns." *International Journal of Mechanical Sciences*, 41(8):995–1019, 1999.

[24]  Shin, K. C., J. J. Lee, K. H. Kim, M. C. Song, J. S. Huh. "Axial crush and bending collapse of an aluminum/GFRP hybrid square tube and its energy absorption capability." *Composite Structures*, 57(1-4):279–287, 2002.

[25]  Mamlouk, M. S., J. P. Zaniewski. *Materials for Civil and Construction Engineers*, 3rd ed., Pearson, 2011.

[26]  Eksi, S., A. O. Kaptiand, K. Genel. "Effects of pre-forming process and PVC foam reinforcement on the deformation behavior of aluminum tube under axial loading." *Acta Physica Polonica A*, 132(3-II):875–878, 2017.

[27]  Yalçın, M. M., K. Genel. "On the axial deformation characteristic of PVC foam-filled circular aluminium tube: Effect of radially-graded foam filling." *Thin-Walled Structures*, vol. 144, 2019.

[28]  OnlineMetals.com. "Aluminum round tube 6061 T6/T6511 products." https://www.onlinemetals.com/en/buy/aluminum-round-tube-6061-t6-t6511.

[29]  ISIS Education Committee. "ISIS education module no. 2: an introduction to FRP composites for construction." *ISIS Canada*, 2006.

[30] Alkhrdaji, T. "Strengthening of concrete structures using FRP composites." *STRUCTURE Magazine*, 2015.

[31] Farley, G. L. "Energy absorption of composite materials." *Journal of Composite Materials*, 17(3):267–279, 1983.

[32] Protech Composites. "About carbon fibers." http://www.protechcomposites.com/what-is-carbon-fiber/.

[33] DragonPlate. "Carbon fiber 101: understanding weaves and fabrics." 2019. https://dragonplate.com/carbon-fiber-101-understanding-weaves-and-fabrics.

[34] Fibre Glast. "What are unidirectional carbon fiber fabrics?" https://www.fibreglast.com/product/What-are-Unidirectional-Carbon-Fiber-Fabrics/Learning_Center.

[35] Elevated Materials. "Carbon fiber weaves: what they are and why to use them." 2019. https://www.elevatedmaterials.com/carbon-fiber-weaves-what-they-are-and-why-to-use-them/.

[36] Simpson Strong-Tie Composite Strengthening Systems. *Technical Data Sheet for CSS-ES*.

[37] Zenkert, D., J. Backlund, S. Smidt, O. T. Thomsen, J. Kepler, A. Kildegaard, O. Schubert, M. Vikstrom, L. Falk, K. Falt-Karlsson, T. Astrom. *The Handbook of Sandwich Construction*, 1997.

[38] Diab Group. *Guideline to Core and Sandwich*.

[39] Thornton, P. H. "Energy absorption by foam filled structures." *SAE Technical Paper Series*, 1980.

[40] Alia, R. A., Z.W. Guan, A. K. Haldar, W. J. Cantwell. "A numerical study of the energy-absorption characteristics of metal polymer foams." *Journal of Sandwich Structures & Materials*, 18(5):597-623, 2016.

[41] Raut, S. V., V. S. Kanthale, B.S. Kothvale. "Review on application of aluminum foam in sound absorption technology." *International Journal of Current Engineering and Technology*, 4:178-181, 2016.

[42] Tiger Foam Insulation. https://tigerfoam.com/sprayfoaminsulation/open-cell-vs-closed-cell-foam-which-should-i-choose/.

[43] Net Composites, 2019. https://netcomposites.com/guide/core-materials/other-foam-cores/.

[44] Diab Group. *Technical Data Divinycell H*.

[45] Sharma Rao N., T. G. A. Simha, K. P. Rao, G. V. V. Ravi Kumar. "Carbon composites are becoming competitive and cost effective." Infosys, 2014.

[46] MetalMiner. "Carbon steel: MetalMiner prices." *MetalMiner*, 2021. https://agmetalminer.com/metal-prices/aluminum/

[47] US Composites. "Epoxy resin and hardener systems." *US Composites*, 2021. http://www.uscomposites.com/epoxy.html

[48] Fiberglass Supply. "Case, 9 sheets, H-80 Divinycell plain." *Fiberglass Supply,* 2021. http://www.fiberglasssupply.com/Product_Catalog/Core_Materials/core_materials.html

[49] American Society of Civil Engineers. "Table C3.1-1a minimum design dead loads (psf)." *Minimum design loads and associated criteria for buildings and other structures: ASCE/SEI 7-16*, pp. 427-428, 2017.